Available online at www.sciencedirect.com
ScienceDirect
Journal of Molecular Structure 798 (2006) 1–26
Journal of MOLECULAR STRUCTURE
www.elsevier.com/locate/molstruc

Feature article

The hidden kernel of molecular quasi-linearity: Quantum monodromy

Manfred Winnewisser [a,*], Brenda P. Winnewisser [a], Ivan R. Medvedev [a], Frank C. De Lucia [a], Stephen C. Ross [b], Larry M. Bates [c]

[a] Department of Physics, The Ohio State University, Columbus, OH 43210-1106, USA
[b] Department of Physics and Centre for Laser, Atomic, and Molecular Sciences, University of New Brunswick, P.O. Box 4400, Fredericton, NB, Canada E3B 5A3
[c] Department of Mathematics and Statistics, University of Calgary, Calgary, AB, Canada T2N 1N4

Received 29 April 2006; received in revised form 14 June 2006; accepted 30 June 2006
Available online 11 September 2006

Abstract

Chain molecules with one low-lying bending mode provide a set of model species for the exploration of quantum monodromy in quasi-linear molecules. Recent work on water [N.F. Zobov et al., Chem. Phys. Lett. 414 (2005) 193–197] and NCNCS [B.P. Winnewisser et al., Phys. Rev. Lett. 95 (2005) 243002.] have shown that the topology of the energy–momentum maps of such molecules follows closely the predictions based on the mathematical concept of non-trivial monodromy. From existing data and new calculations which extrapolate beyond the existing data for several species, we can now present the topological properties of the bending-rotation energy–momentum maps of a range of molecules, from rigidly linear to rigidly bent. The generalized semi-rigid bender (GSRB) Hamiltonian used for the extrapolations is reviewed, and the mathematical concepts required to define the monodromy perspective are presented. Furthermore, it is shown that the energy–momentum map for the end-over-end rotational energy, represented by the effective rotational constant B or $\bar{B}$, has previously unremarked properties which, like the basic bending-rotation energy–momentum map, are robust across the whole set of molecules studied. The molecules discussed are OCCCS, NCCNO, HCNO, OCCCO, ClCNO and BrCNO, NCNCS, HCCNCO, NCNCO and NCSCN.

Keywords: Quasi-linearity; Quantum monodromy; Molecular dynamics; Rotational spectroscopy; Energy–momentum maps

1. Introduction

Very early in the history of quasi-linear molecules it was recognized that the term value intervals between adjacent vibrational bending levels decrease with increasing excitation energy as a bent molecule approaches the energy of the top of the barrier to linearity. In 1964 Dixon [1] recognized further, from NH_2 electronic spectra, that the term value intervals increase again as soon as the molecule passes above the barrier to linearity with increasing excitation. As a result, interesting minima can be seen by plotting the NH_2 term values against K_a. These minima are called the "Dixon dips" and occur just at the top of the barrier. A few years later in 1967 Johns [2] summarized the effects of quasi-linearity in some three-atomic molecules following the formalism proposed by Thorson and Nakagawa [3]. This classic work presents a correlation of the energy levels of a linear molecule with those of a bent molecule. While a linear molecule possesses a two-dimensional, essentially harmonic, potential function, a bent molecule possesses a two-dimensional potential well with a hump in the middle and a circular minimum, but only motion in one of the two dimensions is considered a vibration, and is roughly harmonic. Johns pointed out that although the energy levels correlate smoothly between the two cases, there is a difference between the vibrational quantum number needed for a linear molecule, denoted as v_l, and that relevant for a bent molecule, denoted as v_b. The two sets of quantum numbers

* Corresponding author. Tel.: +1 614 688 8140; fax: +1 614 292 7557.
E-mail address: winnem@mps.ohio-state.edu (M. Winnewisser).

0022-2860/$ - see front matter © 2006 Elsevier B.V. All rights reserved.
doi:10.1016/j.molstruc.2006.06.036

are related by the expression $v_l = 2v_b + |K_a|$. The asymmetric rotor angular momentum quantum number K_a quantizes the projection of the total angular momentum on the axis of least moment of inertia, a, which is an approximately good quantum number in the near-prolate asymmetric rotor. However, in the linear molecule, K_a actually is a good quantum number, representing the vibrationally induced angular momentum along the axis of the molecule, and is identical with $|\ell|$ in the traditional linear molecular model. In 1976 Yamada and Winnewisser [4] extended this work by performing model calculations in order to understand in more detail the correlation between a linear molecule and a bent molecule and to classify the molecules using a quasi-linear parameter that could be empirically determined.

To describe correctly the bending dynamics of the full range of molecules from bent to linear it was found that a Hamiltonian with a reference coordinate system which depends on the large-angle bending coordinate is required, and special measures must be taken to deal with a singularity at the linear configuration. Such a model was introduced in 1970 by Hougen, Bunker, and Johns (HBJ) [5] to treat the vibration–rotation problem in triatomic molecules. The extension of this Hamiltonian to polyatomic quasi-linear molecules will be briefly reviewed in this paper.

It is humbling to note that all the work on molecules exhibiting large-amplitude bending vibrations up to a few years ago, including reviews [6,7], missed the hidden kernel of quasi-linearity, the unifying underlying mathematical property determining the dynamics, namely the quantum manifestation of non-trivial monodromy which must dominate the topological properties of the associated molecular term value maps.

The concept of monodromy (Greek for "once around") is now essential in advanced classical mechanics. In the mathematical realm, geometrical obstructions to global action-angle variables were discussed in 1972 by Nekhoroshev [8]. Duistermaat in 1980 provided an example that brought the subject close to real systems by applying the theory to the spherical pendulum [9]. In 1983 Cushman [10], building on the work of Duistermaat [9], discussed in great detail the geometry of the energy–momentum map of the spherical pendulum, a system which is completely integrable since energy and angular momentum are conserved. As we are now finding out, many other simple physical systems exhibit non-trivial classical or quantum monodromy.

In 1991, Bates [11] gave an example of a completely integrable particle motion in the plane that did not possess a global set of action variables. This example is motion in a circularly symmetric potential shaped like the bottom of a champagne bottle, and hence there is not only a conserved energy, but a conserved angular momentum as well. The punt, or hump, at the bottom of the potential implies, via Morse theory, that the topology of an energy surface bifurcates from one of the topological type of $S^2 \times S^1$ to one of topological type S^3. This change in the topology forces an associated torus bundle to be nontrivial, and hence there cannot be a globally well-defined pair of action variables. In what follows we shall refer to the values of the energy and angular momentum at the top of the potential hump as the critical, or monodromy point.

The translation of the classical notion of monodromy into the quantum domain first appears in 1988 in the work of Cushman and Duistermaat [12], and was given a spectroscopic realization by Child and collaborators [13–15]. Child [14] pointed out via classical trajectory calculations that for a particle moving in a plane in a potential well, the sense of precession below the monodromy point changes sign abruptly if the analogous trajectory lies above the monodromy point. This effect can be related to the fact that for all energy values the outer potential energy wall acts as a concave barrier in configuration space, while the inner potential energy hump presents a convex shape for energies below the monodromy point and no barrier at all for energies above the monodromy point. Thus, the reflection properties of the potential energy walls encountered by the particle change at the classical monodromy point.

Quantum monodromy studies must necessarily be concerned with energy eigenvalues, and this means studying the organization of energy levels and the nature of their dislocation close to the top of the potential barrier in a two-dimensional anharmonic potential well. Not surprisingly, the robust properties of the topology of the potential energy surface are mapped onto the energy–momentum map and thus into the rovibrational spectra of quasi-linear molecules. In the present work, the manifestations of quantum monodromy for real champagne bottle potentials will be discussed.

The publications on this subject so far have treated only the patterns observed in the spectrum associated with the two degrees of freedom describing the bending of a molecule. However, there are two more degrees of rotational freedom, with quanta smaller than the bending quanta, but coupled, as we shall see, with the bending motion; these are the two components of the end-over-end rotation of a molecule, about its b and c principal axes. We will present the energy–momentum plot of the two primary bending degrees of freedom in one plot, and the end-over-end energy in a separate plot; the two energy contributions are roughly additive, especially near the linear limit.

The remainder of the paper is organized as follows: In Section 2, we review the implications of the correlation diagram between a linear and a bent molecular model. In this context, we introduce ten molecules with bending potential functions which span most of that range. Section 3 presents a brief review of the current version of the General Semi-Rigid Bender (GSRB) Hamiltonian. Section 4 deals with the monodromy calculation for a champagne bottle potential and the monodromy matrix. Section 5 presents each of the ten model molecules and the perspective given by their energy–momentum maps. New data on NCNCS are used to show the effect of monodromy on the $K_a = 1$ splitting. A concluding discussion follows in Section 6.

2. The correlation between linear and bent molecules

Our concepts of molecular structure are determined by the potential surfaces of molecules. A linear molecule is linear because it has a deep, roughly parabolic cylindrically symmetric bending potential function. A bent molecule is bent due to a deep potential well, roughly parabolic in the radial coordinate, about an equilibrium angle which is comfortably far from the linear configuration. In both cases the bending motion upon vibrational excitation may be considered to be infinitesimal. So we have a word, in each of the two limiting cases, that contains all that information. However, there is a fairly large number of molecules – much larger than thought as the phenomenon was originally defined – that we call quasi-linear, because the bending motion is *not* infinitesimal, the potential function is very anharmonic, may have a hump, and moderate excitation (2, 10, or 20 quanta) may take the energy levels above that hump. We wish to treat this whole set of molecules with one formalism; nature certainly does. The simplest way to do this is to draw a correlation diagram, in which we can follow energy levels with a given set of quantum numbers from the linear limit to the bent limit or vice versa. This is done in Fig. 1. The upper part of the diagram shows model calculations for a triatomic two-dimensional rigid bender, meaning that the stretching vibrations are ignored and the end-over-end rotation is omitted by taking $J = K_a$. A parabolic potential well is taken for the linear limit on the left side, with the fundamental bending quantum ν_0 as the unit of energy. A Gaussian hump is added, which becomes progressively larger across the diagram. The term values for the linear case are thus $E/(hc\nu_0) \approx (v_l + 1)$, whereas those for the right hand limit shown are $E/(hc\nu_0) \approx (v_b + 1/2) + AK_a^2/(hc\nu_0)$ [4].

The most important reason for showing this figure (yet again) is that it is not intuitively easy to follow the transition of a vibrational degree of freedom over into a rotational degree of freedom. While the linear molecule has a degenerate bending mode, that is with two vibrational degrees of freedom (one in the plane, one perpendicular to it; they can also be defined in polar coordinates), the motion of both determined by the potential function, the bent molecule is described as having a non-degenerate, one-dimensional bending motion. The depicted curve is the one-dimensional or radial potential function for that bending motion, and the other dimension, out of the plane, is considered to be a rotational degree of freedom, with the motion determined by the inertial properties of the molecule. Our classification of these degrees of freedom is based on the Born-Oppenheimer-type separation of vibration and rotation, which works well at both limits of the range but *does not work* in the transitional region. The potential curves shown are in each case a radial cut through the two-dimensional cylindrically symmetrical potential for the two degrees of freedom under consideration, regardless of their classification.

By following a few of the lower excited levels across the diagram, one can get a feel for the transition. The first excited state of the linear molecule, on the left in Fig. 1 at $E \approx 2hc\nu_0$, has the vibrational quantum number $v_l = 1$ and the (vibrational) angular momentum quantum number $\ell = 1$. When we follow this state across the diagram, this level retains the value of its angular momentum quantum number, though we are familiar with calling it K_a for the bent case, which quantizes the projection of the total (rotational) angular momentum along the axis of least moment of inertia. This, then, is a conserved quantity and a good quantum number, and we may use K_a and ℓ interchangeably for this discussion. This level is, however, in the vibrational state $v_b = 0$ for the bent limit: v is not a good quantum number except in the two limiting cases.

If we take the level of the linear molecule with $v_l = 2$ and $\ell = 0$, and follow it across the diagram, we see that it retains the value of $\ell = K_a = 0$, but it reveals itself in the bent limit as the lowest rotational level of the $v_b = 1$ or first excited vibrational state of the bent molecule. This shows us the expression relating v_l and v_b:

$$v_l = 2v_b + |K_a| \quad \text{or} \quad v_b = (v_l - |\ell|)/2. \tag{1}$$

The physical basis for this relation is that if the two-dimensional vibrational wave equation for the linear molecule is solved in cylindrical coordinates, then the eigenvalues of the radial wave equation have the quantum number $n = v_b$.

The quasi-linear parameter shown in the lower part of Fig. 1 was devised in order to classify molecules according to an empirical measure of how far away they are from one limiting case or the other. The most practical measure that was found, that combines the effects of the masses of the atoms, the force constants of the potential well and the height of the barrier, is the ratio γ of the intervals between the ground state and the two levels followed in the above discussion,

$$\gamma = \frac{\Delta E(\ell = 1)}{\Delta E(\ell = 0)} = \frac{E(v_l = \ell = 1) - E(0)}{E(v_l = 2, \ell = 0) - E(0)} \tag{2}$$

or

$$\gamma = \frac{\Delta E(K_a = 1)}{\Delta E(K_a = 0)} = \frac{E(v_b = 0, K_a = 1) - E(0)}{E(v_b = 1, K_a = 0) - E(0)}, \tag{3}$$

where the intervals $\Delta E(\ell)$ or $\Delta E(K_a)$ are shown in Fig. 1.

This ratio is seen to have the values 1/2 for the linear limit, and, in the bent limit, assuming a Born–Oppenheimer separation, near 1/100. To make the scale nearly symmetric, we use for the quasi-linearity parameter, somewhat arbitrarily,

$$\gamma_0 = 1 - 4\gamma. \tag{4}$$

The energy of the lowest excited state with $K_a = 1$ is given roughly in the bent limit by the value of the A rotational constant, since the bent molecule is a near-prolate asymmetric rotor. As the molecule is made more linear, the A constant becomes larger; this corresponds to the increase in this quantum as one moves to the left in the diagram.

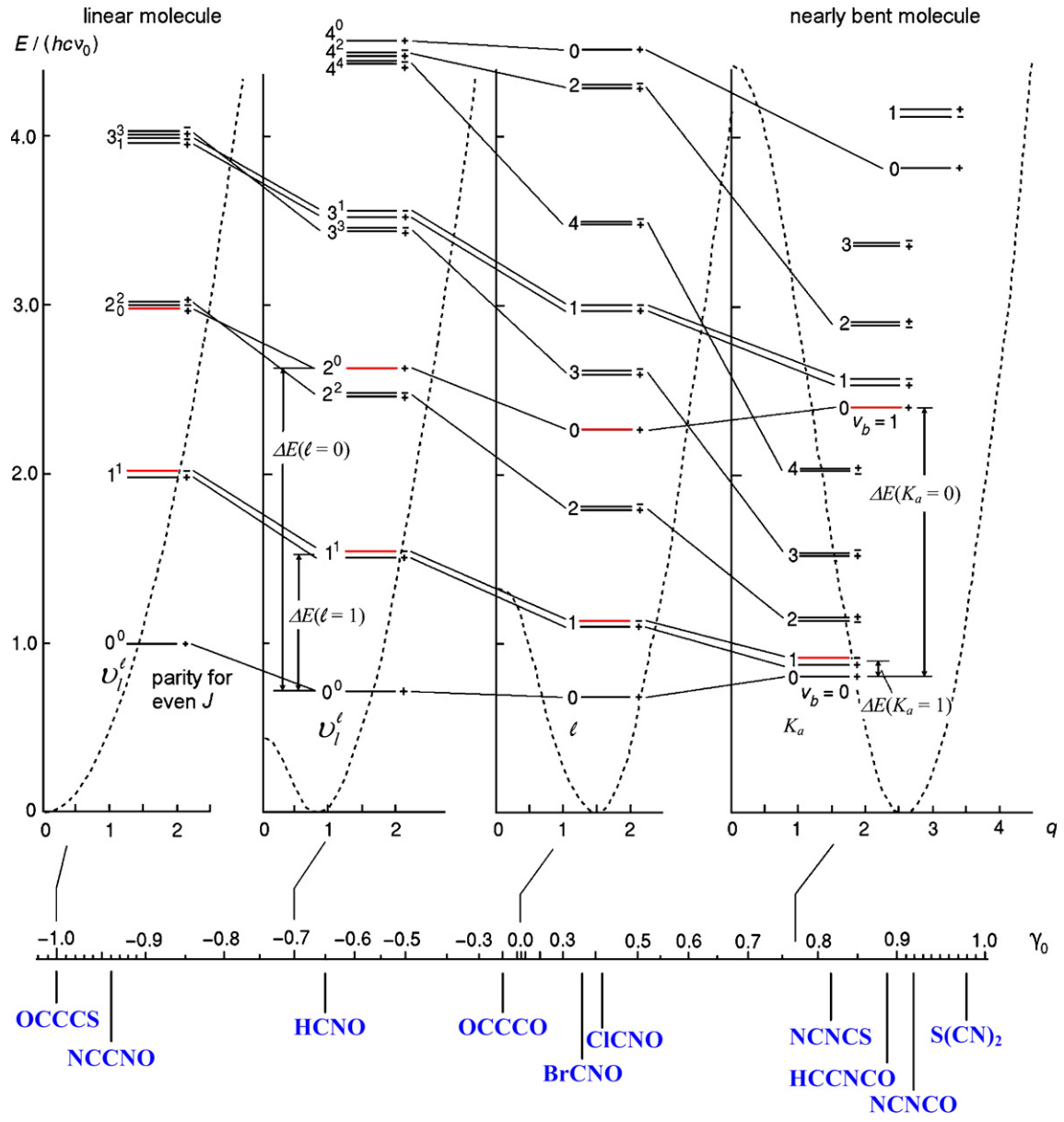

Fig. 1. Correlation between the bending-rotation energy levels of linear and bent triatomic molecules, drawn from model calculations [4]. The potential functions are given by $V = hc\nu_0(\frac{1}{2}q^2 + \alpha e^{-\beta q^2})$ with $\ln(2\alpha\beta) = 1.5$ where α and β are dimensionless parameters that determine the shape of the potential and q is a dimensionless coordinate which represents displacement from the linear configuration. v_l is the vibrational quantum number of a linear molecule, and the superscript (or small label) ℓ refers to the vibrational angular momentum. ℓ corresponds in the bent limiting case, where the vibrational quantum number is v_b, to K_a, the quantum number of the rotational angular momentum component about the axis of least moment of inertia. Molecules discussed in this paper are located as indicated on the scale of the quasi-linearity parameter γ_0.

But it does not go towards infinity at the linear configuration, as it would if the Hamiltonian for an asymmetric rotor were used: instead it goes over into the vibrational energy quantum ν_0 in the linear limit. Away from either limit, this quantum has both vibrational and rotational character; *there is no good separation of variables*.

At the bottom of Fig. 1, a selection of chain-form molecules are entered on the γ_0 scale. Each of these molecules exhibits one large-amplitude bending mode, connecting otherwise nearly rigid linear groups of atoms. The remaining vibrational modes are considerably higher in energy, so that these species offer spectra in which the energy manifold associated with the low-lying bending mode, corresponding closely to a simple curvilinear valence bending coordinate, can be studied without major complications due to interactions with other vibrations. The large-amplitude mode of each of these molecules has been shown to have a potential function and an energy level distribution corresponding to the indicated position of the molecule on the γ_0 scale. The existing literature on their spectra, supplemented by new calculations and new measurements for one of them (NCNCS), are used in this work to illustrate the insights on this class of molecules granted by the new perspective based on the concept of quantum monodromy.

We will use primarily the conventional notation for bent molecules because the quantum mechanical Hamiltonians that have proved capable of reproducing the energy levels of such systems across the entire range are those that use the lower symmetry of the bent case.

3. The General Semi-Rigid-Bender (GSRB) Hamiltonian

The Semi-Rigid Bender (SRB) Hamiltonian of Bunker and Landsberg [16] is one of the variations derived from the original HBJ Hamiltonian [5]. Appropriate for the rotation–vibration of a molecule possessing a single large-amplitude vibration, the complete rigid bender model is a four-dimensional Hamiltonian with one vibrational degree of freedom describing the bending of an otherwise rigid molecular framework, and three rotational degrees of freedom. The SRB model extends the rigid bender model by allowing for relaxation of the molecular framework (stretching) as it undergoes large-amplitude motion. The SRB can be viewed as either an extension of the rigid bender model or as an approximation to the nonrigid bender of Hoy and Bunker [17]. In its derivation a curvilinear bending coordinate was introduced representing the large-amplitude bending vibration, and two rectilinear stretching coordinates. This Hamiltonian could be used for any triatomic molecule. The initial work incorporating relaxation due to the stretching modes included only one rotational degree of freedom [16]. To account for molecular end-over-end rotation, Bunker and Stone [18] extended the previous theoretical work. Although rigorous and detailed non-rigid models for a triatomic molecule with a large-amplitude bend have been developed, such as the model of Hoy and Bunker [17], the Morse Oscillator Rigid Bender Internal Dynamics (MORBID) Hamiltonian [19] and the variational calculations that have been very successful with H_2O [20], it is feasible but not yet practical to use them for more than four atoms. The SRB concept, however, can be extended to model the dynamics of any chain molecule with a particularly low-lying bending mode, and to reproduce most of the features of the spectra of such molecules, even if experimental accuracy cannot quite be achieved. The list of molecules to be discussed, specified in the lower part of Fig. 1, shows that for this collection of data we need a model that can handle a quasi-linear molecule with 4–6 atoms. We have therefore remained with the level of approximation of SRB calculations. As will be seen, the parameters that can be derived are physically informative and have predictive value.

The SRB is described in Refs. [16,18,21]. The large-amplitude coordinate, ρ, is the supplement of the valence angle. The reference configuration employed for the Hamiltonian depends on this angle. Therefore, at the core of the SRB treatment is a ρ-dependent four-dimensional extended moment of inertia matrix. This matrix, its inverse, and various derivatives (potentially up to the third derivative) with respect to ρ, are needed in the calculations. In much SRB work these quantities are recalculated for each different molecular geometry and thus for each different modeling of the large-amplitude bending motion, sometimes requiring a prodigious amount of algebra and code. However, it is possible to reformulate these quantities, *algebraically*, in terms of the Cartesian coordinates of the nuclei and the derivatives of these coordinates with respect to ρ [22]. This reformulation, the General Semi-Rigid Bender (GSRB) Hamiltonian, does not depend on the number of atoms in the molecule, can be used for planar or non-planar molecules, and can also be applied to large-amplitude motions other than bending vibrations, for example torsional motions. To date the GSRB program has been used to study the large-amplitude bending motion of chain molecules of various lengths; HSiF [23], HNCO [24], HNCS [25], ClCNO and BrCNO [26], OCCCS, NCNCS, NCNCO, and NCNNN [22], NCCNO [27], HCCNCO [28], and HC_5N [29]; the inversion motion in H_2S_2 [30,31]; the large-amplitude bending motion of the HF moiety in H_2CO–HF [32]; and the "pinwheel" motion in SiC_2 [21].

In order to use the GSRB program for a particular molecular system two subroutines must be supplied: one to specify the Cartesian coordinates of the nuclei and their derivatives for each value of the large-amplitude coordinate, and one to provide the potential energy function for the large-amplitude motion. The moment of inertia matrix is built from molecular internuclear distances and bond angles whose values and variation with ρ are specified by input parameters. For the molecules of concern here these geometric quantities were defined as power series in ρ or $(\rho - \rho_e)$, where ρ_e is the equilibrium value of ρ, either full, even, or odd series, as appropriate.

In the present work, three types of potential function were used:

For the molecules OCCCS, NCCNO and HCNO the potential is written as a power series of even terms in ρ,

$$V(\rho) = \frac{1}{2} f_{\alpha\alpha}\rho^2 + \frac{1}{24} f_{\alpha\alpha\alpha\alpha}\rho^4. \tag{5}$$

The constant $f_{\alpha\alpha}$ may be either positive or negative, in the latter case defining a hump. The quartic force constant $f_{\alpha\alpha\alpha\alpha}$ is small in a molecule close to the linear limit, but when there is a negative quadratic force constant, the quartic constant has been found to define the outer wall of the potential function. This potential has given the best fits for molecules with no hump or only a small hump at the linear configuration.

For the molecules OCCCO, BrCNO, ClCNO, NCNCS, HCCNCO and NCNCO a modified quartic potential well with a Lorentzian hump proposed by Barrow, Dixon and Duxbury [33] was used,

$$V(\rho) = \frac{H(1 + c\rho^2) f_{\alpha\alpha}(\rho^2 - \rho_e^2)^2}{f_{\alpha\alpha}\rho_e^4 + [8H(1 + c\rho^2) - f_{\alpha\alpha}\rho_e^2]\rho^2}, \tag{6}$$

where H is the height of the potential hump, ρ_e the non-zero equilibrium value of ρ, $f_{\alpha\alpha}$ in this case is the quadratic

force constant at ρ_e, and the parameter c adjusts the anharmonicity around the minimum of the potential well.

For $S(CN)_2$, because it is so close to the bent limit, the GSRB calculations were made by fitting eight adjustable anchor points of a cubic spline function about ρ_e; the barrier height could not be obtained from the pure rotational data available. Since the equilibrium internuclear distances were held fixed in the fitting, the potential function is only very approximately determined. A full fitting would have fewer potential parameters and would fit the equilibrium internuclear distances; the geometry and potential are strongly correlated due to the currently limited data.

SRB models, including the present version of the GSRB, do not fully account for higher order effects such as ℓ-type doubling in linear molecules or centrifugal distortion, since these are determined to a large extent by the force field of the stretching modes. This strongly limits the range of J values for which the SRB can reasonably be used when fitting directly to transition frequencies. Various approaches to mitigating this deficiency have been used. One approach is to simply use the calculated low-J rotational energy levels to determine effective rotational constants for individual K_a sublevels of vibrational states and use these to extrapolate to higher J values. Another approach has been to remove the effective centrifugal distortion from the experimental data (rather like 'de-perturbing' a spectrum), before fitting the SRB model. This can be done by obtaining B-values from the experimental data and fitting to these with an SRB [34]. Another approach has been to add ad hoc ℓ-type doubling [22] or centrifugal distortion terms to the SRB Hamiltonian [35]. In the present work we have combined the addition of an ad hoc ℓ-type doubling with the determination of low-J based rotational constants to provide useful information up to $v_b = J = 10$.

For determining the structural and/or potential function parameters of a molecule from a spectrum, the parameters are determined by non-linear least squares fitting to experimental data. The number of parameters that can be determined varies with the nature and amount of data available. The most important parameters, which can almost always be determined except in a few extreme limiting cases, are the two dominant potential parameters, which determine the height of the barrier and the outer potential wall, the internuclear distances of one or both of the bonds adjacent to the pivot atom, and the relaxation (semi-rigid) parameters of one or more of those bonds. In addition the relaxation with bending (semi-rigidity) of some of the other internuclear distances and bond angles can often be determined, along with equilibrium values of some of these internuclear distances and bond angles. Because of the strong coupling of rotation and bending in quasi-linear molecules, it is possible to determine the potential function very reliably from pure rotational data alone if the molecule is well away from either limit.

4. Monodromy calculation for the champagne bottle potential

This section represents an attempt to make the mathematics of monodromy accessible to a wider audience of spectroscopists, to augment previous treatments [11,13,36,37] and to indicate its importance in understanding the spectra of quasi-linear molecules. We first briefly review the mathematical description of the situation (see also Refs. [38–40] for more advanced details).

We endeavor to show monodromy in the champagne bottle potential by examining the trace of motions in configuration space, that is, in the two-dimensional space of the position variables x, y. Consider the classical motion of a particle of unit mass in the xy-plane under the influence of the potential, $V(r)$,

$$V(r) = r^4 - r^2, \tag{7}$$

where $r^2 = x^2 + y^2$ as usual. This potential is shown in Fig. 2. It has a smooth w shape in cross-section and is rotationally symmetric about the origin, which is at the top of the quadratic hump. Somewhat fancifully, this potential is called the champagne bottle due to the hump in the bottom. Continuing the oenological analogy we will, on occasion, refer to the hump as a punt which represents the indentation in the base of a wine bottle. More details may be found in Refs. [11,39].

Let p_x and p_y denote the linear momenta of the particle in the x and y directions. Then, as is customary in classical mechanics, we may write the equations of motion of the particle in first order form as

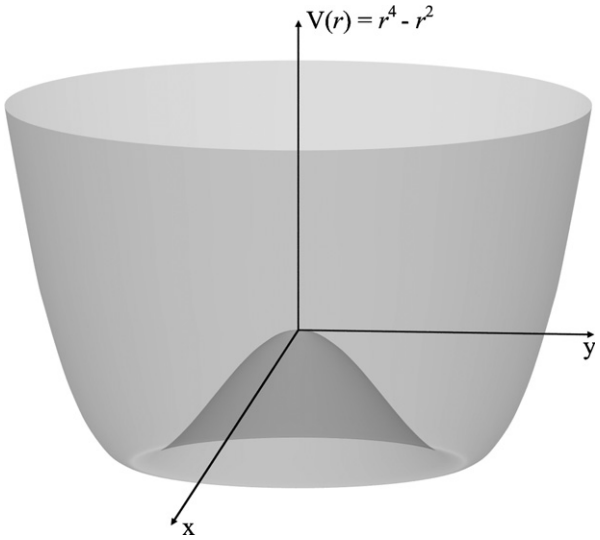

Fig. 2. Champagne bottle potential function $V(r)$ with $r^2 = x^2 + y^2$. The origin of the coordinate system is at the critical point on top of the potential hump. The space below the critical point has the surface topology $S^2 \times S^1$ and above S^3. Therefore no set of global action-angles variables can exist.

$$\dot{x} = p_x,$$
$$\dot{y} = p_y, \tag{8}$$
$$\dot{p}_x = -2x[2(x^2+y^2)-1],$$
$$\dot{p}_y = -2y[2(x^2+y^2)-1]. \tag{9}$$

These differential equations possess two first integrals: the angular momentum j and the energy h. They are

$$j = xp_y - yp_x, \tag{10}$$
$$h = \frac{1}{2}(p_x^2+p_y^2) + (x^2+y^2)^2 - x^2 - y^2. \tag{11}$$

This follows from the fact that the forces are derived from a potential that is rotationally invariant. Consequently, in phase space (the four- dimensional space of position and momentum variables x, y, p_x, p_y) the integral curves of the differential equations of motion (*i.e.* the trajectories) lie on the intersection of the two three-dimensional surfaces in phase space defined by $j =$ constant and $h =$ constant. When convenient we will also use polar coordinates (r, θ) in configuration space and the related natural phase space coordinates $(r, \theta, p_r, p_\theta)$. Now, as can be shown, the typical intersection of these two surfaces is a two-dimensional surface with the topological type of a torus (a surface without boundary) and we are interested in how all the tori fit together. Each pair of values of j and h defines a separate torus such as that shown in Fig. 3. The analogy to keep in mind now is a family of line segments over a circle: a family of (short) vertical segments over a horizontal circle forms a cylinder. However, if the family of segments has a half-twist (from vertical-up around to vertical-down), they form a Möbius band instead. This is what we want to determine: do the integral curves of the differential equations of motion form a set of tori with a twist, or not? In the case of the champagne bottle system, it is difficult to visualize as we have a two-parameter family of tori in four-dimensional phase space. It turns out that a gross topological measure of this fundamental property may be found simply by looking at how the tori fit together when their energy and angular momentum are related by $j^2 + h^2 = a^2$, a a constant. This of course defines a circle of radius a about the origin, the point where $j = h = 0$ in the space spanned by j and h.

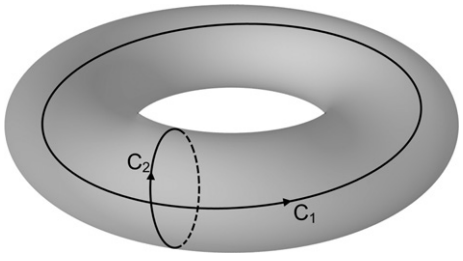

Fig. 3. Each pair of values of j (angular momentum) and h (energy) defines a separate torus in phase space (x, y, p_x, p_y). Each point on the torus surface is determined by two angle coordinates, ϕ_1 and ϕ_2. c_1 and c_2 represent two independent loops on a torus.

Imagine picking two independent loops on a torus (more precisely, a basis for the first homology) as illustrated in Fig. 3, and *moving them from torus to torus* (that is, from trajectory to trajectory, each characterized by its values of j and h), in a continuous fashion, as you traverse the circle $j^2 + h^2 = a^2$.

It is a topological fact that looping around the energy-angular momentum circle $j^2 + h^2 = a^2$ in increments need not have c_1 and c_2 come back to themselves, but they will come back to some integral linear combinations of themselves: this transformation, or product of a series of transformations, is represented by a 2×2 matrix M

$$M = \begin{pmatrix} a & b \\ c & d \end{pmatrix}, \tag{12}$$

where a, b, c, d are all integers and the determinant $ad - bc = \pm 1$. M is the *monodromy matrix* and measures the twist in how all the tori fit together. Since the matrix M depends on the choice of the basis $\{c_1, c_2\}$, we are actually only interested in M up to similarity, *i.e.* $M' = PMP^{-1}$ for $P \in GL(2, \mathbb{Z})$, so that M' is a matrix with integer entries as well. However, it follows that if M is not the identity matrix, then the bundle of all the tori is twisted, just like the Möbius band.

The following section will show that the monodromy matrix M for the champagne bottle problem may be written as

$$M = \begin{pmatrix} 1 & 0 \\ 1 & 1 \end{pmatrix}, \tag{13}$$

and hence that the bundle of all the tori is globally twisted. As we discuss in Sections 4.2 and 4.3, this has dramatic implications for the ordering of rovibrational energy levels in linear chain molecules possessing a potential energy surface similar to that in Fig. 2.

4.1. Explicit calculation of the monodromy matrix

Each torus corresponding to given values of j and h sitting in four-dimensional phase space projects to an annulus in the configuration space centered at the origin under the projection map $(x, y, p_x, p_y) \to (x, y)$. The map from the torus to the annulus is a two-to-one map for points away from the boundary of the annulus, and this corresponds to whether or not the radial momentum p_r is positive or negative.

We now consider the effective potential and how it determines the radii of the inner and outer boundaries of the annulus in our champagne bottle problem. Suppose we are given a Hamiltonian of a particle in a rotationally invariant potential of the form

$$h(q,p) = \tfrac{1}{2}|p|^2 + V(|q|) \tag{14}$$

and let $r = |q|$. Here $q, p \in \mathbb{R}^n$, where we typically think of $n = 2$ or 3. Since the potential is rotationally invariant, the angular momentum J is conserved. Let $j = |J|$, and write

the Hamiltonian equations of motion in polar coordinates. The equation for the radial momentum p_r is

$$\dot{p}_r = -\frac{\partial h}{\partial r}, \tag{15}$$

and because of the conserved angular momentum, we may substitute out p_θ *etc.* to get

$$\dot{p}_r = -\frac{\mathrm{d}V}{\mathrm{d}r} + \frac{j^2}{r^3}. \tag{16}$$

The important point here is that this equation may be considered as a Hamiltonian equation of motion for the one degree of freedom Hamiltonian

$$h_j(r, p_r) = \tfrac{1}{2}p_r^2 + V_j(r), \tag{17}$$

where $V_j(r) = V(r) + \frac{j^2}{2r^2}$. $V_j(r)$ is called the *effective* or *amended* potential, and it is best to think of it as a family of problems depending on the parameter j. From the symmetry/reduction viewpoint, we would say that the reduction of the full problem by the rotation group has yielded a reduced problem, *that is still Hamiltonian*, and the reduced Hamiltonian is h_j. This is a special case of a general theory of reduction of Hamiltonian systems with symmetry. Perhaps a more physical viewpoint is to think of an observer sitting at the origin in a frame corotating with the particle and observing only the radial part of the motion. The observer then sees the radial motion as described by the one degree of freedom Hamiltonian with the amended potential. Roughly speaking, the potential has to be amended to account for the non-zero angular momentum acting as a barrier so that the particle cannot reach the origin.

To make things perhaps more concrete, let's run through the explicit calculation for the champagne bottle: in polar coordinates the Hamiltonian is

$$h(r, \theta, p_r, p_\theta) = \frac{1}{2}\left(p_r^2 + \frac{1}{r^2}p_\theta^2\right) + r^4 - r^2 \tag{18}$$

and so the Hamiltonian equations of motion are

$$\dot{r} = p_r \tag{19}$$

$$\dot{\theta} = \frac{1}{r^2}p_\theta \tag{20}$$

$$\dot{p}_r = -4r^3 + 2r + \frac{p_\theta^2}{r^3} \tag{21}$$

$$\dot{p}_\theta = 0 \tag{22}$$

Now the last differential equation says that $p_\theta =$ constant, which we will call j (it is of course the angular momentum). Substituting this constant value into the differential equation for p_r, we find

$$\dot{p}_r = -4r^3 + 2r + \frac{j^2}{r^3} = -\frac{\mathrm{d}V_j(r)}{\mathrm{d}r} \tag{23}$$

with

$$V_j(r) = r^4 - r^2 + \frac{j^2}{2r^2} \tag{24}$$

as you would expect from the theory. For a given value of h_j and j, one can find the minimum and maximum values of r (here we are thinking of finding the boundary radii of the annulus) by setting $p_r = 0$ into the reduced Hamiltonian

$$h_j(r, p_r) = \frac{1}{2}p_r^2 + r^4 - r^2 + \frac{j^2}{2r^2}. \tag{25}$$

This yields a sixth order polynomial for r, which is cubic in $s = r^2$:

$$2s^3 - 2s^2 - 2h_j s + j^2 = 0. \tag{26}$$

With a (very) little calculus you can show that this polynomial has three real roots for $j \neq 0$, and precisely two of them are positive. If $j = 0$, then the conclusion still holds if $h < 0$, except that the third root is now equal to zero.

The inner and outer boundaries represent the minimum and maximum values of the radial coordinate r in the amended or effective potential $V_j(r) = r^4 - r^2 + j^2/(2r^2)$. Thus even for $h > 0$, the projection for $j \neq 0$ is still such an annulus. These boundaries for $j \neq 0$ are only bounds to the value of r and should not be confused with cross-sections of the champagne bottle potential.

Let us now consider a trace on the torus and to describe it in terms of loops, such as c_1 and c_2 in Fig. 3. Now a loop is a type of a cycle and in the projection of a torus shown in Fig. 4 we let $\alpha^{\pm}$, $\beta^{\pm}$ be a basis for cycles on the torus in phase space. We choose $\beta^{\pm}$ so that they represent pure radial motion, and $\alpha^{\pm}$ so that they represent pure angular motion. Plus or minus signs are assigned depending on whether or not the angular momentum is positive ($j > 0$) or negative ($j < 0$). A pair consisting of one α cycle and one β cycle is a basis for the fundamental group of the torus.

A common way of picking the loops and moving them continuously, as described in the previous subsection, is to compute local action-angle variables (I_1, I_2, ϕ_1, ϕ_2)

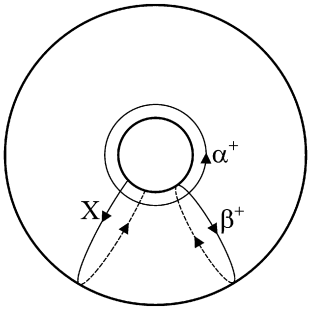

Fig. 4. For $j > 0$ and $h < 0$ (but close to 0) the projection under the map π: $(x,y,p_x,p_y) \to (x,y)$ takes a phase space torus (Fig. 3) to an annulus in configuration space with inner and outer boundaries. α^+ represents a cycle over which we integrate $p_\theta\,\mathrm{d}\theta$, β^+ represents a cycle over which we integrate $p_r\,\mathrm{d}r$. X represents the flow of the Hamiltonian vector field (*i.e.* a trajectory) for an oscillating particle in the potential trough between the outer (concave) and inner (convex) potential walls. Solid curves represent $p_r > 0$, while the dashed curves corresponds to $p_r < 0$. In the case of $h < 0$ we see that $\lim_{j \downarrow 0^+} X = \beta^+$, indicating that the integral curve of X looks like β^+.

and letting c_1 be the oriented loop that corresponds to $\phi_2 =$ constant and similarly for c_2. ϕ_1 can then be used as a parameter on the loop c_1 with the orientation of the loop given by the direction of increasing ϕ_1; similarly for c_2 and ϕ_2. In the case at hand we make the concrete choice of actions by letting $I_1^{\pm} = j$, which corresponds to the integral of $p_\theta \, d\theta$ over the loops α^+ or α^-, and $I_2^{\pm}$ be the integral of $p_r \, dr$ over the loops β^+ or β^-. More precisely, the action $I_1^{\pm} = j$ is everywhere, and the actions $I_2^{\pm}$ may be analytically continued. The actions $I_2^{\pm}$ are locally real-analytic functions, and so there is no ambiguity in analytically continuing them in any simply-connected domain. Furthermore, it is crucial to keep in mind that these are local constructions which are *not* valid when the angular momentum $j = 0$.

We let X denote a loop in an integral curve of the equations of motion, in other words a single trajectory, and consider its properties in various regions of the energy–momentum space. We first consider the case of negative energy (*i.e.* below the top of the punt displayed in Fig. 2) but still close to zero, say $h = -\varepsilon$. Imagine a motion of the particle with slightly positive angular momentum $0 < j \ll 1$. If the particle starts at the inner boundary of the annulus, it will move with increasing r until it hits the outer boundary, and then return. All the while, it will be moving in such a way that the angle θ is slowly increasing. To summarize, the particle moves so that it is oscillating back and forth in the potential trough while the angle slowly increases. We draw one cycle of this motion in Fig. 4.

Note that when the energy is negative, $h < 0$, then taking the limit as the angular momentum j tends to zero from above, $\lim j \downarrow 0^+$, means that the trajectory or integral curve X looks more and more like the loop β^+.

Reversing the sign of the angular momentum so that $j < 0$, as shown in Fig. 5, the situation is almost identical, and taking the limit as the angular momentum j tends to zero from below, $\lim j \uparrow 0^-$, the trajectory or integral curve X looks more and more like the loop β^-. Combining this negative energy case with the previous one we see that β^+ and β^- meet at the limit $j = 0$, that is,

$$\beta^- = \beta^+ \text{ for negative energy.} \tag{27}$$

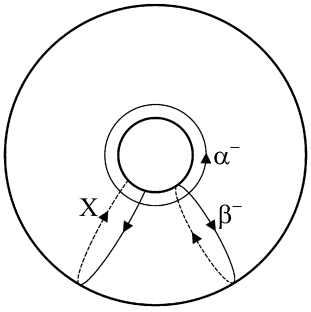

Fig. 5. As the previous figure (Fig. 4) for $h < 0$, but with $j < 0$. α^- and β^- are the labels of the cycles for $j < 0$. For $h < 0$ we see that $\lim_{j\uparrow 0^-} X = \beta^-$, indicating that the integral curve of X looks like β^-.

We now consider positive energy, for which the picture is slightly different. This is shown in Fig. 6. If the angular momentum were zero, the particle would shoot straight across the punt, and have an angular change of π as it moved across the potential well. However, we need to draw this when the angular momentum is positive, but still close to zero. Now we see that in the limit $j \downarrow 0^+$, $\beta^+ = X - \frac{1}{2}\alpha^+$. This is most easily seen by dilating α^+ out to the outer boundary of the annulus, which we may do since it represents a homology class. Here we should recall the following definition: two curves are homologous if their difference forms the boundary of a surface. In our case, the surface is an annulus. Hence, any circle of constant radius in the annulus is homologous to any other having the same orientation. Since it is clear that the curve α^+ can be deformed to the outer boundary by continuous dilation, the two curves α^+ and the outer boundary are homotopic. Since the two curves are homotopic, they represent the same homotopy class, and hence the same homology class.

For negative angular momentum we have the limit $j \uparrow 0^-$, $\beta^- = X + \frac{1}{2}\alpha^-$, as can be seen in Fig. 7. Combining this positive energy case with the one above, we see that $\beta^+ + \frac{1}{2}\alpha^+$ meets $\beta^- - \frac{1}{2}\alpha^-$, so that

$$\beta^- = \beta^+ + \tfrac{1}{2}\alpha^+ + \tfrac{1}{2}\alpha^- \quad \text{for positive energy.} \tag{28}$$

Some calculation shows that the energy–momentum map from the phase space $\mathbb{R}^4$ to $\mathbb{R}^2$ given by $(x,y,p_x,p_y) \to (j,h)$ can take values in the j, h plane given by

$$(j = \pm\sqrt{4r^6 - 2r^4},\ h \geqslant 3r^4 - 2r^2), \tag{29}$$

where $r \geqslant 2^{-1/2}$ is the radial coordinate in $\{x,y\}$ space.

The boundary of this image is shown by the solid curve in Fig. 8, with only the region above the curve being physically accessible. Region 1 is below the monodromy point while region 2 is above. Every point of regions 1 and 2 that is not on the boundary of the image and not at the origin is a regular value, and the inverse image of every regular point in the image is a torus in four-dimensional phase space.

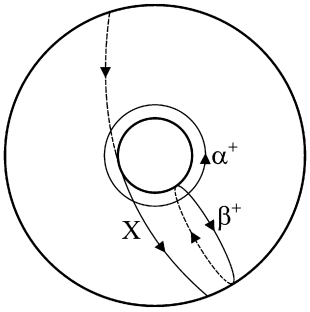

Fig. 6. As Fig. 4 with $j > 0$ but now with $h > 0$ (but close to 0). Here the oscillating particle has energy above the hump and only encounters the outer (concave) potential wall. For positive energy $h > 0$ and positive $j > 0$, $\lim_{j\downarrow 0^+} X = \beta^+ + \frac{1}{2}\alpha^+$ if α^+ is dilated to the outer boundary of the annulus, which indicates that the integral curve of X looks like β^+ with $\beta^+ = X - \frac{1}{2}\alpha^+$.

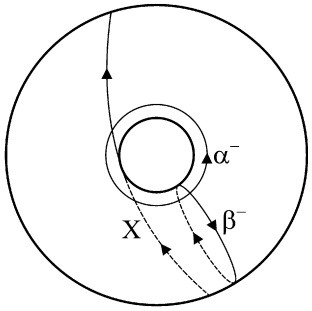

Fig. 7. As the previous figure (Fig. 6) for $h>0$ but now with $j<0$. For positive energy $h>0$ and negative $j<0$, $\lim_{j\uparrow 0^-} X = \beta^- - \frac{1}{2}\alpha^-$, which indicates that the integral curve of X looks like β^- with $\beta^- = X + \frac{1}{2}\alpha^-$ if α^- is dilated to the outer boundary of the annulus.

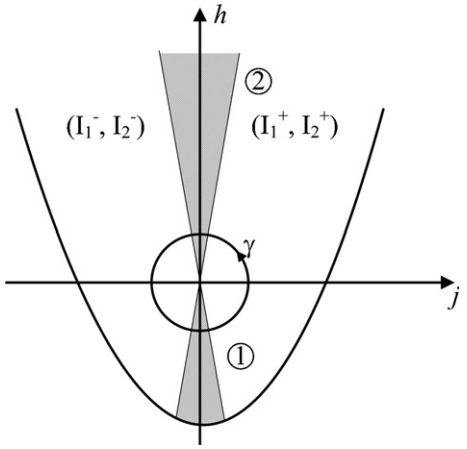

Fig. 8. Image of the energy–momentum map for the champagne bottle potential. The actions $I_1^{\pm}$ and $I_2^{\pm}$ are defined as $I_1^{\pm} = \int_{\alpha^{\pm}} p_\theta \mathrm{d}\theta$ and as $I_2^{\pm} = \int_{\beta^{\pm}} p_r \mathrm{d}r$ where the $-$ sign corresponds to $j<0$ and the $+$ sign to $j>0$. Region 1 is below the monodromy point while region 2 is above. γ denotes a loop enclosing the critical point. The shaded regions are where the continuations of the action variables may be compared. The transition maps for the actions in region 1 and 2 differ and are given in Eqs. (30) and (31).

The inverse image of each boundary point is a circle. Each one of these points when $j\neq 0$ represents a circular orbit in the phase space, which occurs when the angular momentum is extremized for a given energy. The lowest point in the image also has as inverse image a circle, but represents the points where the particle is at rest in the bottom of the potential well. The inverse image of the origin is a pinched torus, which may be viewed as the torus in Fig. 3, with the loop c_2 collapsed to a point. This pinched torus represents all the trajectories whose limiting position is the origin as time $t\to\pm\infty$. The pinch point is of course where the particle sits in unstable equilibrium at the top of the punt.

Since the pair of cycles $\{\alpha^-,\beta^-\}$ are only well-defined when the angular momentum is negative, and the cycles $\{\alpha^+,\beta^+\}$ are only well defined when the angular momentum is positive, we can use the results of the above limiting argument to see how they are related in the regions labeled 1 and 2 of Fig. 8. This enables us to say what happens to the cycles when we traverse the loop γ in j,h space once in the positive (counterclockwise) sense. In both regions 1 and 2, $\alpha^+ = \alpha^-$. That $\alpha^+ = \alpha^-$ globally is due to the fact that α is an integral curve of the action of the rotation group. This is a free action on the set of regular values of the energy–momentum map. In Eqs. (27) and (28) above we found the relationship between β^- and β^+ in both regions. Combining this information we find that in region 1

$$\begin{pmatrix}\alpha^+\\ \beta^+\end{pmatrix} = \begin{pmatrix}1 & 0\\ 0 & 1\end{pmatrix}\begin{pmatrix}\alpha^-\\ \beta^-\end{pmatrix} \tag{30}$$

while in region 2

$$\begin{pmatrix}\alpha^-\\ \beta^-\end{pmatrix} = \begin{pmatrix}1 & 0\\ 1 & 1\end{pmatrix}\begin{pmatrix}\alpha^+\\ \beta^+\end{pmatrix}. \tag{31}$$

The monodromy map is just the product of the two transition maps from region 1 to 2 and back again. From this we conclude that what happens to the tori as we move around the loop γ is

$$M = \begin{pmatrix}1 & 0\\ 1 & 1\end{pmatrix}. \tag{32}$$

As stated above, this means that the bundle of all tori is twisted. We shall see the consequences of this in Sections 4.2 and 4.3, below. The preceding calculation is technically simple, but largely hides a crucial geometric fact. That is, when the torus has positive energy and zero angular momentum, its projection into the configuration space is not an annulus, but a disc. The map is no longer two-to-one, because there is an entire circle of points on the torus that project to the origin of configuration space. Hence, the limit of the cycles β^+ and β^- is not well-defined. However, the limit of the Hamiltonian dynamics is well-defined, and that is why we make the calculation in the way that we do.

4.2. Vector interpretation of determining monodromy

There is another interpretation of monodromy in classical mechanics that may help the reader visualize the quantum case. Recall that the action variables are constant on the tori, and so may be viewed as functions on the image of the energy–momentum map. Their independence means further that the actions define local coordinates in the energy–momentum space. From the coordinate lines $I=$ constant we may construct a frame of vectors that we may move in a parallel fashion. Here parallel is defined as *looking parallel in the action coordinates*. Moving the frame around the set of regular values defines a notion of parallel transport that is locally path independent, but need not be globally so. This notion of parallel transport is globally well-defined even though the action variables are only locally defined, because of the restrictions on the transition maps between local sets of action variables. If there is no global parallelism, we say that the torus bundle has

monodromy. More details of this point of view may be found in [11]. The quantum analogue of this is to view the lattice of spectral points as having a defect. We have not stressed this interpretation in this paper as it is far harder to see the moving frame in the dynamics of the particle motion.

4.3. Quantum Monodromy

The connection between classical and quantum mechanics is given by the quantization rule that says that the wave functions will have support on those tori for which the actions are an integral multiple of $2\pi\hbar$ (for the sake of this discussion we are ignoring the Maslov correction). This quantization rule is independent of the choice of local actions because the actions in overlapping regions may be taken to be related to each other by a linear transformation in $GL(2,\mathbb{Z})$. This quantization rule gives us a set of local quantum numbers, which depend on the choice of actions. In particular, we get a direct correspondence between the non-existence of global action variables, and the non-existence of a global set of quantum numbers that describe the system. It is in this sense that we refer to the lattice of quantized action variables as possessing a defect. A full discussion of the details of the quantum constructions may be found in [45, 46].

Inspecting Fig. 1 we see that the molecules BrCNO, ClCNO, NCNCS, HCCNCO and NCNCO each must have vibrational states below the critical point in the potential function. If such a quasi-linear molecule experiences sufficient thermal excitation, then the higher lying bending states become more and more populated. In the classical picture we could say the molecule can traverse the potential hump and thus has an unstable linear configuration at the critical point. In the classical realm such an unstable equilibrium is called a focus-focus singularity [36,47,48]. Integrable quantum systems with two degrees of freedom and a focus-focus singularity, like our champagne bottle potential, will exhibit non-trivial quantum monodromy [47].

In the quantum realm the continuous energy–momentum map given in Fig. 8 is replaced by the quantum lattice of the system [13–15] as mentioned above. Fig. 9 displays a part of the image of the quantum lattice energy–momentum map for the molecule NCNCS (discussed later in Section 5.6, below) which has a champagne bottle potential for its large-amplitude bending mode ν_7. In this quantum lattice, the interpretation given in Section 4.2 becomes convenient to visualize. In this figure we move a unit cell **a** spanned by the two column vectors $(\Delta K_a, \Delta v_b) = (0, 1)$ and $(\Delta K_a, \Delta v_b) = (1, 0)$ around the critical point (which is located near $K_a = 0$ for $v_b = 3$ and is indicated in the center of Fig. 9 as a black star). The parallel evolution of the two vectors (see Section 4.2) on an anticlockwise circuit starting at **a** and proceeding around the monodromy point to **g** shows that the vector (0,1) returns to itself while the vector (1,0) becomes (1,1). Thus, exactly as the pair of cycles $\{\alpha,\beta\}$ are skewed by the monodromy matrix of Eq. (32) during

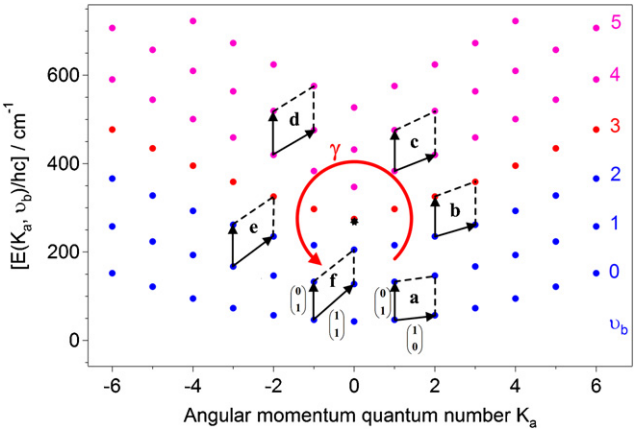

Fig. 9. Partial image of the quantum lattice energy–momentum map for the molecule NCNCS which has a champagne bottle potential for the bending mode ν_7. Bent vibrational notation is given on the right hand side. Blue dots represent term values for v_b for which the $K_a = 0$ points lie below the monodromy point. The red dots are the series of term values just above the monodromy point. The classical monodromy point is indicated by a black star which is located near the term value for $K_a = 0$, $v_b = 3$. The two column vectors $(\Delta K_a, \Delta v_b) = (0, 1)$ and $(\Delta K_a, \Delta v_b) = (1, 0)$, indicated at unit cell **a**, are transported in parallel fashion counterclockwise (red circle) around the critical point. By following the path γ from unit cell **a** to unit cell **f** around the monodromy point we clearly see that vector (0,1) returns to itself while vector (1,0) becomes vector (1,1). The transformation matrix for the vectors is the monodromy matrix given in Eq. (32).

the counterclockwise motion around the loop γ in the classical Fig. 8, the unit cell column vectors in the quantum case of Fig. 9 are skewed by the identical monodromy matrix during the equivalent counterclockwise loop γ in the quantum diagram. The clockwise transport is effected by the inverse of this matrix. The take-home message is that there is no global vibrational quantum number: below the monodromy point v_b is justified as such, *i.e.* it is a local quantum number (blue dots in Fig. 9) while above the monodromy point the linear notation with v_l is more appropriate. A more detailed discussion of the properties of the energy–momentum map of NCNCS is offered in Section 5.6.

Since only the energy and the angular momentum are conserved physical quantities of the system, only K_a remains a good quantum number. Due to the existence of classical monodromy there exists in the quantum lattice of the energy–momentum map no global regularity and therefore, as mentioned above, neither v_b nor v_l are good *global* quantum numbers. Thus quantum monodromy can be interpreted as a lattice defect which causes a robust dislocation of energy states [49] and constitutes an intrinsic property of the molecular quantum system.

5. Quasi-linear molecules, their structures, two-dimensional potential wells and energy–momentum maps

From a dynamical point of view all the chain-form molecules which will be discussed in this section have one common physical property, namely the existence of a low-lying

bending vibration well separated from the rest of the other normal modes, which are all above 400 cm^{-1}. As mentioned before, these molecules with their equilibrium structures span the entire range from a truly linear molecule to a truly bent molecule.

Quasi-linear molecules are found to have structural parameters (internuclear distances and bond angles) that do not allow us to assign to them a single Lewis structure or any clear-cut carbon bond hybridization scheme. The punt in the champagne bottle potential function (the barrier to linearity) of these molecules is the residual of a difference between two (or more) large energy contributions arising from a balance between different electron correlation effects [42]. For simplicity, we represent the molecular structures in the following subsections using the notation for the dominant bonding scheme among the relevant resonance structures. For details of the data and calculations on which the plotted geometrical quantities are based, and discussions of the structures in each case, the reader is referred to the original publications on each molecule.

The importance of the rotational constant B associated with end-over-end rotation in quasi-linear molecules was recognized in the work of HBJ [5], and considerable effort was expended in that and other work to quantify it. The range of molecules considered was not broad enough at that time to reveal the basic features of the evolution of this constant with v_b and K_a. It is indeed important, and is the major novel focus of this work. The angular momentum quantized with K_a can be separated, in first order, from the end-over-end rotation in the linear limit, but in a real, bent molecule it is one of three coupled rotational degrees of freedom. The more bent a molecule becomes, the less the end-over-end rotation can be separated from the rotation about the a axis.

As a measure of the end-over-end rotation, we take an effective rotational constant defined for each value of K_a and v_b; thus we will call it $B(K_a,v_b)$, obtained for linear or nearly linear species as the first coefficient in a simple polynomial fit in $J(J+1)$ to the corresponding series of energy levels for successive J values. For species closer to the bent limit, the levels which correlate with those just specified for the linear case give us a value of $B(K_a, v_b) \equiv \bar{B} = (B+C)/2$, again for each value of K_a and v_b. For this presentation we will average any resolvable asymmetry splitting or ℓ-type doublets, in particular for $K_a = 1$ and 2. As noted above, in the bent limit the rotational degrees of freedom cannot be cleanly separated, and with increasing asymmetry K_a no longer has the properties of a good quantum number. However, in the range of what we generally term a near-prolate rotor ($\kappa < -0.9$), the definition given here is still a useful indication of the distribution of rotational energy. The coupling of the end-over-end rotation with the large-amplitude bending-rotation motion will be seen to be significant.

Although the potential function can be considered complete if plotted just for positive ρ, we want to show a cut through the entire two-dimensional coordinate space considered in the rigid bender Hamiltonian, and we thus plot the curve for azimuth 0 and π as $E_{pot}(\rho,Azimuth)$. This corresponds to the energy/momentum plots mapped from the spectrum, which are derived from the general classical case in which positive and negative K_a can be distinguished, and in particular allows the differentiability of the curves connecting the energy levels, in the patterns produced by the mapping, to be easily seen.

The information is presented for each molecule in a sequence which follows the perspective of the analysis of rotationally resolved spectra. We first propose a model for the structure, and then derive effective parameters from the spectrum, such as a set of $B(K_a,v_b)$ values, and look for trends. This is the assignment phase. Only after such trends are understood can the quantitative analysis of the spectrum be iteratively extended and, with the appropriate (effective) Hamiltonian, completed. For many of the molecules discussed, the trends observed were very perplexing. Earlier, we just went on to fit the spectrum as best we could, without fully seeing what all the anomalies meant; now we know we can make an energy–momentum plot using $B(K_a,v_b)$ values to gain insight into the dynamics directly. A full analysis using the GSRB allows us to determine the potential function and also the bending-rotation levels, if not already measured, for all but very bent species. The potential curve was the final stage of our analysis, previously. We now take this one step further with the bending-rotation energy/momentum plot, which grants us immediate insight into the systematics of the dislocation of energy levels and the resulting complexities of the spectra.

The color scheme is the same for each plot and each molecule: states with the same value of v_b as the $K_a = 0$ state closest to the monodromy point are plotted in red; states with a higher v_b (all states if there is no monodromy point) are plotted in pink; and states with a lower v_b are plotted in blue. States with a common v_b are connected by blue, red or pink lines; states with a common v_l are connected by green lines.

As in Fig. 1, we start with the linear limiting case. The effects of monodromy emerge as we work our way across the range of γ_0 from -1 to $+1$.

5.1. Tricarbon oxide sulfide, OCCCS

The experimental data for OCCCS were obtained from microwave [51,52], millimeter wave [53–55], and infrared measurements [56], high-resolution Fourier transform measurements in the far-infrared [57], and Doppler-limited terahertz spectroscopy [58]. Panel (a) in Fig. 10 shows the clearly linear equilibrium structure. The potential function resulting from GSRB calculations based on the data is shown in panel (c) together with the bending vibration energy levels, in the traditional presentation form. The lowest bending term value of 77.4 cm^{-1} guarantees that the ν_7 bending mode is well separated from all the other normal vibrational modes. The ν_7 bending manifold can be

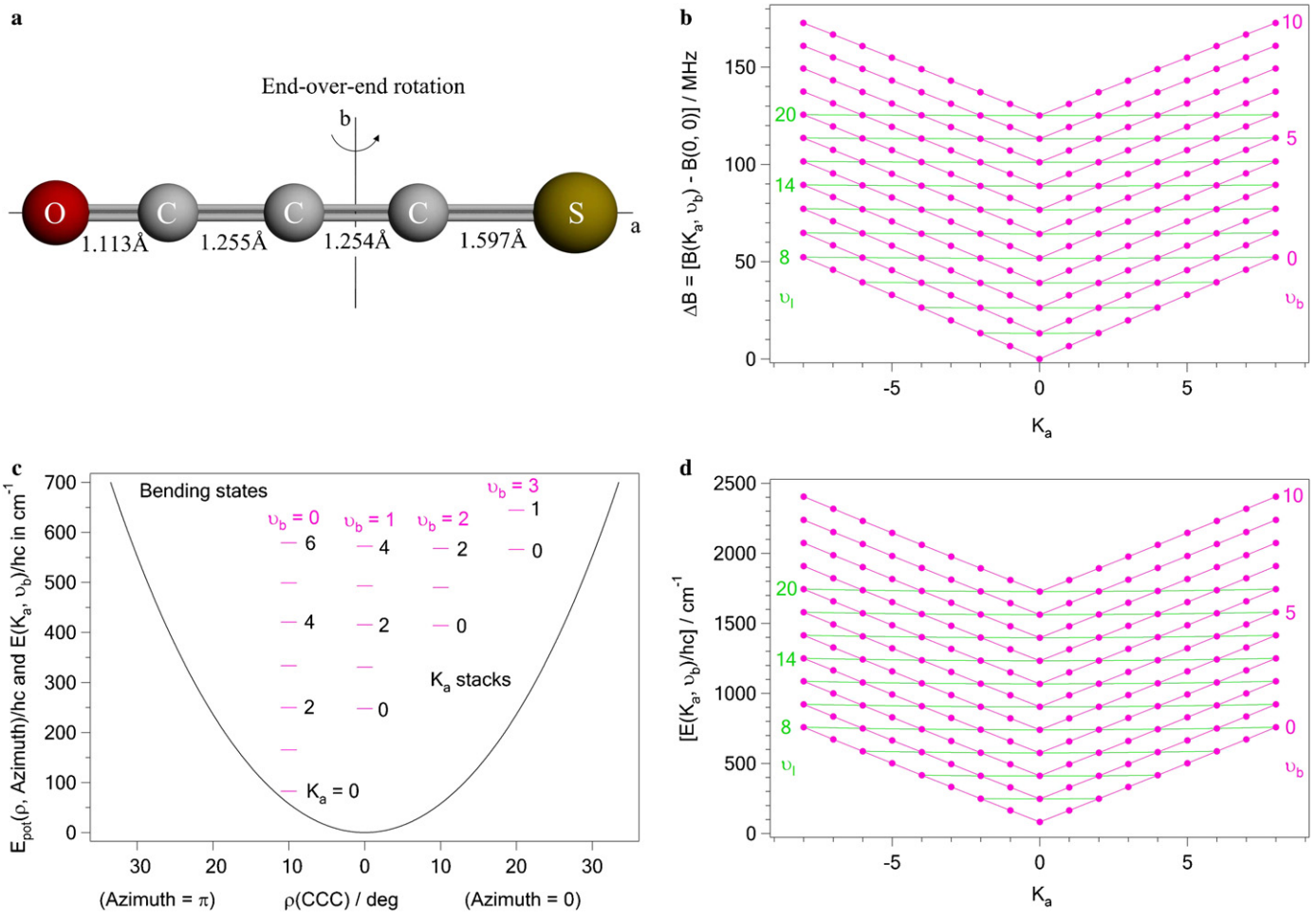

Fig. 10. (a) The structure of OCCCS (GSRB parameters [22]) in the principal axis system [50]; (b) end-over-end rotational contributions to the energy plotted as ΔB versus K_a; (c) the radial bending potential function for ν_7 [22]; and (d) the two-dimensional bending-rotation term values for $J = K_a$ plotted versus K_a. Points plotted for $v_l \leqslant 8$ and $K_a \leqslant 8$ are experimentally determined; higher levels are calculated with the GSRB.

described successfully by the model of a very nearly harmonic two-dimensional isotropic oscillator [22]. The potential function shown in Fig. 10 panel (c) is given by Eq. (5), and the quadratic and quartic force constants are given in Table 1. The molecular structure parameters derived via the isotopic substitution method [50] were used for starting parameters and were fixed for the parameters that could not be determined in the GSRB calculation [22]. The r_s/GSRB structure of OCCCS is that displayed in panel (a) of Fig. 10. The conserved physical quantities are energy

Table 1
Potential parameters used in the calculations of the various potential functions for the molecules to be discussed

Molecule	$f_{\alpha\alpha}$/cm^{-1} rad^2	$f_{\alpha\alpha\alpha\alpha}$/ cm^{-1}rad^4	H/cm^{-1}	c/rad^{-2}	ρ_e/rad	References
OCCCS	3758.0[a]	11954.0				[22]
NCCNO	1493.9[a]	23007.4				[27]
HCNO[b]	−602.4[a]	47373.6				[34,41]
OCCCO	915.7[c]		18.3	1.475	0.421	[42]
BrCNO	4083.3[c]		130.8	−0.044	0.479	[26]
ClCNO	4755.4[c]		166.9	−0.051	0.501	[26]
NCNCS	3578.6[c]		270.9	−0.048	0.681	[22,43]
HCCNCO	5864.9[c]		537.2	−0.092	0.686	[28]
NCNCO	6927.9[c]		1014.8	−0.044	0.884	[22]
$S(CN)_2$	56434.2[c]		29000.0		1.417	[44]

[a] Force constant defined at the linear configuration.
[b] The original quadratic force constant has been multiplied by 2 and the original quartic constant by 24 in order to make these constants compatible with the other entries in this table and Eq. (5).
[c] Force constant defined at the minimum ρ_e of the champagne bottle potential.

and angular momentum and they are presented in two complementary diagrams, the form of which is chosen for the whole set of molecules in order to identify any signature of quantum monodromy. In panel (a) of Fig. 10 the axis of the end-over-end rotation is indicated by b. The rotational energy is represented by the effective rotational constant $B(K_a,v_b)$, for convenience shown as $\Delta B = [B(K_a,v_b) - B(0,0)]$ versus K_a; that is, the change in the $B(K_a,v_b)$ value from the ground state value due to the bending-rotation motion is shown. In panel (d) of Fig. 10 the bending-rotational term values $E(K_a,v_b)/hc$ of states with zero end-over-end rotation but including rotation about the axis of least moment of inertia, thus with $J = K_a$, are plotted versus K_a. This is the total energy associated with the two degrees of freedom required to describe the bending dynamics.

The two energy–momentum plots resemble each other for OCCCS very closely. It should be noted that each bending-rotation state is represented in these plots as a point in a phase space. The connecting straight lines represent the groupings defined by two possible assignment notations for vibrational states: linear notation (green color) and bent notation (pink color). The identical form of these two plots, like an idealized ladder diagram [60], show that the OCCCS molecule can be considered a poster species for the linear molecular model. Lines connecting states of the same vibrational state, in the linear notation, are smooth, indeed quite straight; lines drawn relevant for the bent notation are all discontinuous at $K_a \equiv \ell = 0$. All of these geometrical or topological properties are characteristic for a linear molecule, or a quantum harmonic oscillator.

5.2. Cyanofulminate, NCCNO

The molecular structure of NCCNO was first determined by high-resolution Fourier transform microwave spectroscopy [62] and used in the GSRB calculations [27] which led to the potential function displayed in Fig. 11 panel (c). The low-lying central CCN bending mode of NCCNO was characterized by rotational spectroscopy in the millimeter wave and sub-millimeter wave range as well as by high resolution ro-vibrational spectroscopy in the far infrared range [27]. The term value of the first excited state

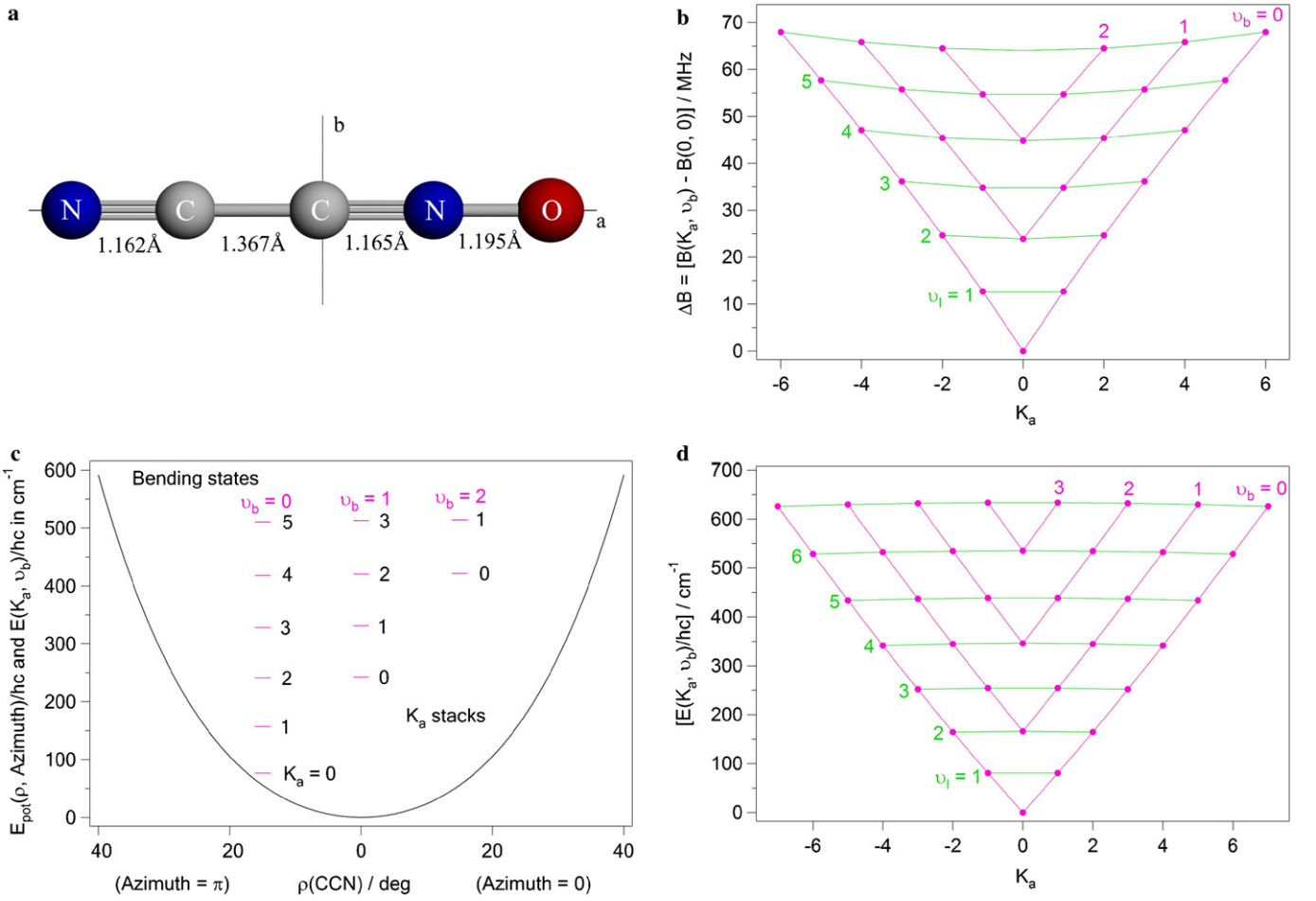

Fig. 11. (a) The structure of NCCNO (GSRB parameters [27]) in the principal axis system; (b) end-over-end rotational contributions to the energy plotted as ΔB versus K_a; (c) the radial bending potential function for ν_7; and (d) the two-dimensional bending-rotation term values for $J = K_a$ plotted versus K_a. All points plotted represent experimental data.

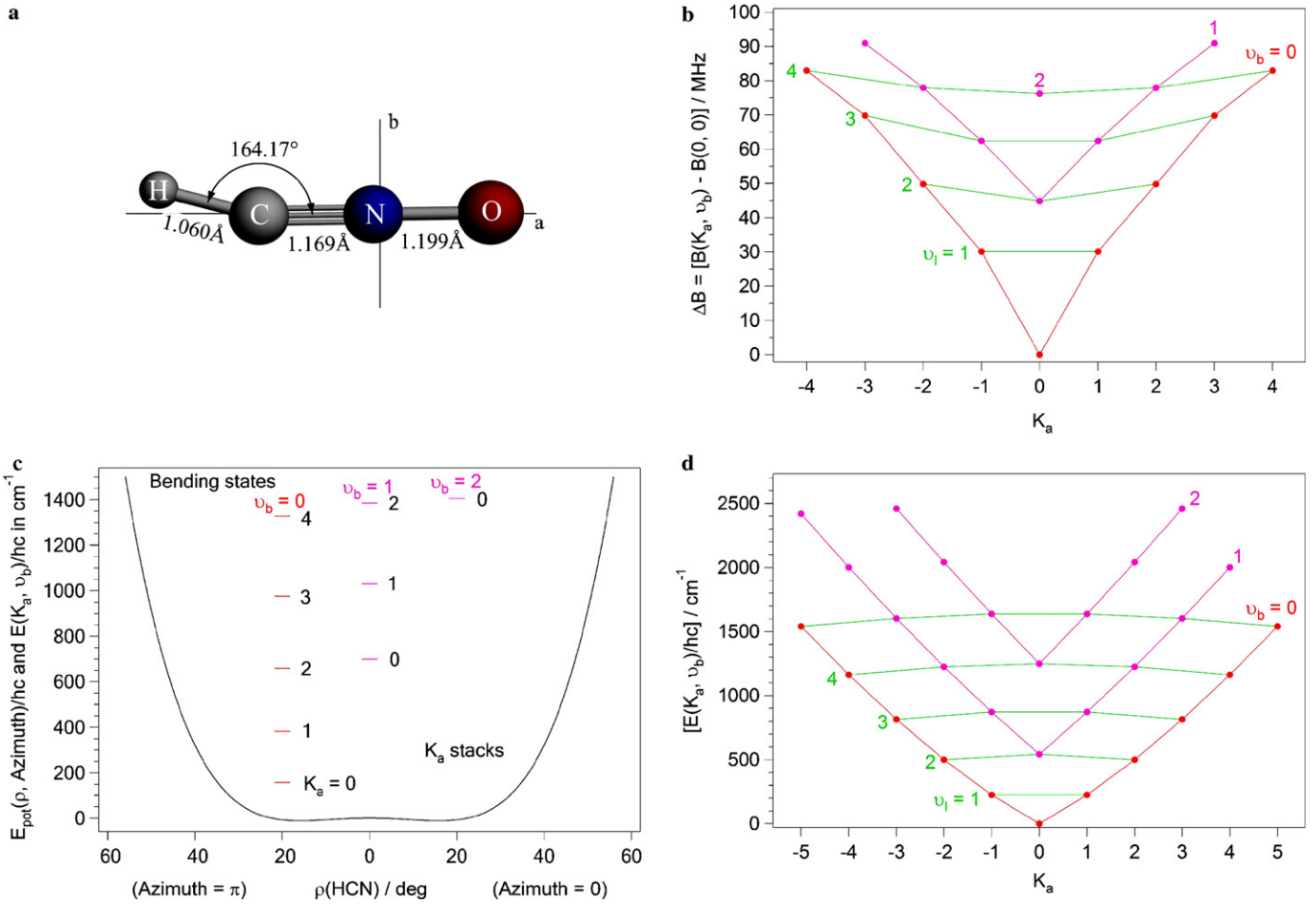

Fig. 12. (a) The structure of HCNO in the principal axis system (substitution [63] and SRB [34,41] parameters); (b) end-over-end rotational contributions to the energy plotted as ΔB versus K_a; (c) the radial bending potential function for ν_5 [34]; and (d) the two-dimensional bending-rotation term values versus K_a for $J = K_a$. All points plotted represent experimental data.

of the bending mode was found to be 80.524 cm^{-1} so that it is well separated from all other vibrational modes. The GSRB analysis of the rotational and far infrared data [27] provides us with an effective CCN bending potential function given by Eq. (5) that has a minimum at the linear configuration. From Table 1 it is seen that the quartic contribution is substantial, but the quadratic term is clearly positive. Thus no critical point can exist in the potential surface. However, a curvature of the lines connecting the ΔB values in panel (b) and term values in panel (d) of Fig. 11 can be observed: the quartic term in the potential function causes a slight curvature of the green (linear notation) and pink (bent notation) lines which is opposite in the two plots.

5.3. Fulminic acid, HCNO

HCNO is the simplest of the nitrile oxide family of molecules, and has been extensively studied because of its quasi-linear properties [59,64–67]. In contrast to the previous molecule, it has an effective bending potential function, for the large-amplitude vibration, that is essentially quartic with a small but negative quadratic contribution [34,41]. The conventional resonance structures are $H–C{\equiv}N^{\oplus}–O^{\ominus} \leftrightarrow H–C^{\oplus}{=}N{=}O^{\ominus}$; deuterium substitution supports the identification of the lower bending mode as the predominantly HCN large-amplitude bend. Eq. (5) represents the potential function with force constants listed in Table 1. The height of the potential hump in the bottom of the potential well as shown in Fig. 12 (c) is 12 cm^{-1}, well below the lowest ground state $K_a \equiv \ell = 0$ energy level. The effective potential function derived from the bending-rotation energy levels is not identical to the equilibrium potential which was calculated *ab initio* in 1996 [68,34], since zero-point contributions of the small-amplitude vibrational modes increase the barrier height. Up until that time, the determination of an accurate *ab initio* structure of fulminic acid was a real challenge to quantum mechanical methods, because depending on the theoretical method and level of calculation, the calculated barrier height varied from zero to several hundred reciprocal centimeters. The situation was even worse for calculating the term value of the fundamental excitation of the large-amplitude HCN bending vibration [69].

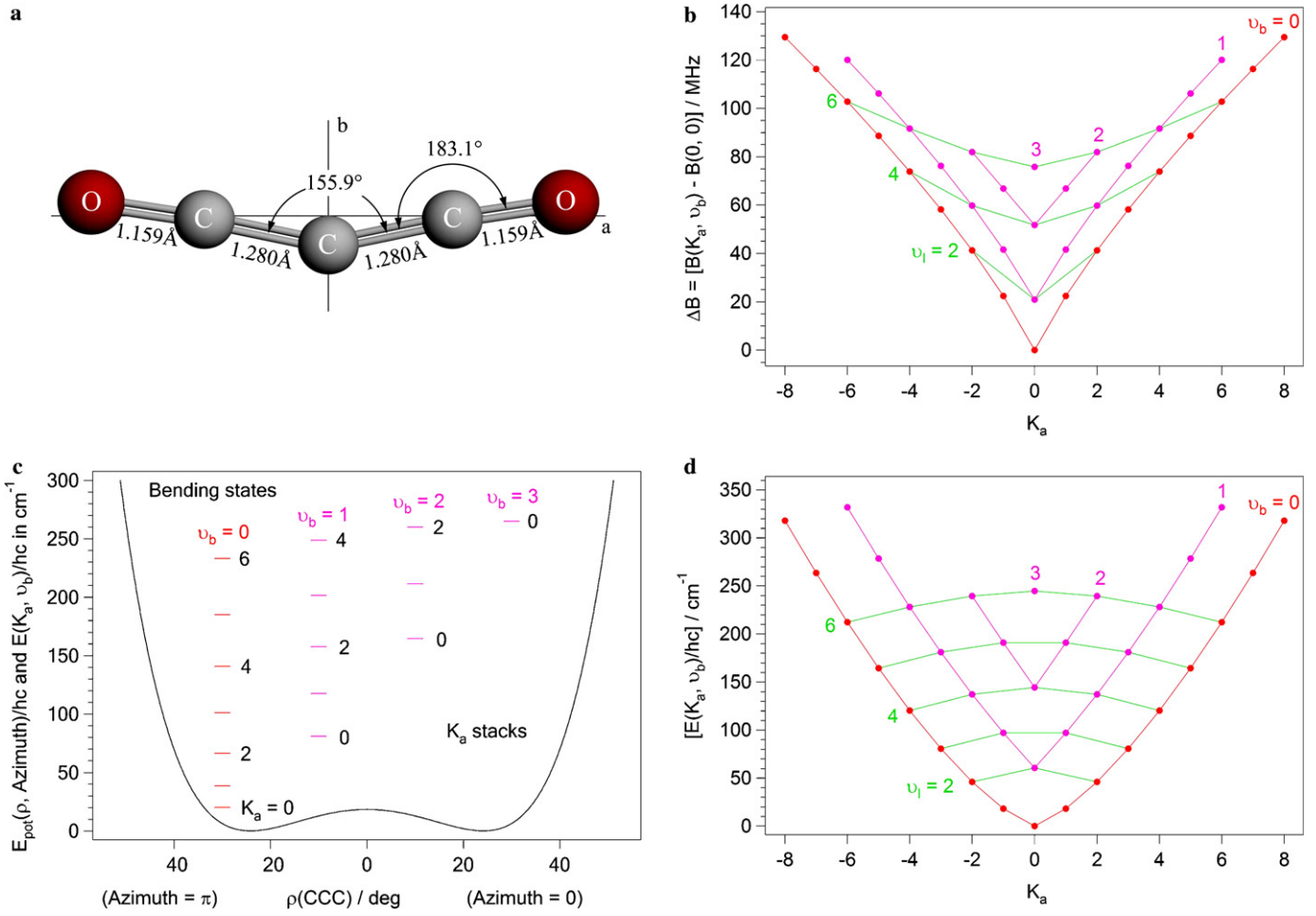

Fig. 13. (a) The structure of OCCCO (*ab initio* parameters [42]) in the principal axis system; (b) end-over-end rotational contributions to the energy plotted as ΔB versus K_a; (c) the radial bending potential function for ν_7 of OCCCO [42]; and (d) the two-dimensional bending-rotation term values $E(K_a,v_b)/hc$ plotted versus K_a for $J = K_a$. All data plotted are experimentally determined and can be found in Ref. [61].

The experimental term value was determined to be 224.10 cm^{-1}.

The very modest hump in the potential surface due to the negative quadratic term suffices to define a critical or monodromy point. Therefore the curvature of the green (linear notation) and pink (bent notation) curves connecting the points in both energy–momentum maps, especially the exaggerated kink at the ground state $K_a = 0$ point, mark the onset of quantum monodromy, even though there are no states below the critical point of the potential function. Although the semi-rigid bender model [34,41] has greatly contributed to our understanding of the rovibrational dynamics of the HCNO molecule, it cannot reproduce the rotational and vibrational energy levels within experimental accuracy. However, entire networks of anharmonic resonance systems in the spectra of HCNO were built up using the Ritz combination principle [65,70]. The physical reason for this situation is not only the HCN large-amplitude motion with the onset of quantum monodromy, visible in the energy–momentum maps, but also the fact that the other vibrational modes are not well separated from the HCN bending mode. The CNO bending mode is located at 537.18 cm^{-1} while the lowest stretching mode has a term value of 1254 cm^{-1}. Upon excitation of any of the three stretching modes, the effective potential which can be determined for the HCN bending mode changes significantly [34].

5.4. Tricarbon suboxide, OCCCO

Among quasi-linear molecules tricarbon suboxide is historically outstanding. Starting in 1935 extensive spectroscopic work, electron diffraction studies and theoretical calculations tried to illuminate the conflicting experimental results: is this molecule now linear or bent at the central carbon atom as depicted in panel (a) of Fig. 13? For the chemists and spectroscopists at that time it was difficult to imagine that an either/or decision, linear or bent, was simply not appropriate. The revealing history of this enormous scientific effort and conceptual struggle to understand the structure, dynamics, and bending potential function for OCCCO is summarized in Ref. [6]. With the advent of modern high-resolution sub-millimeter wave

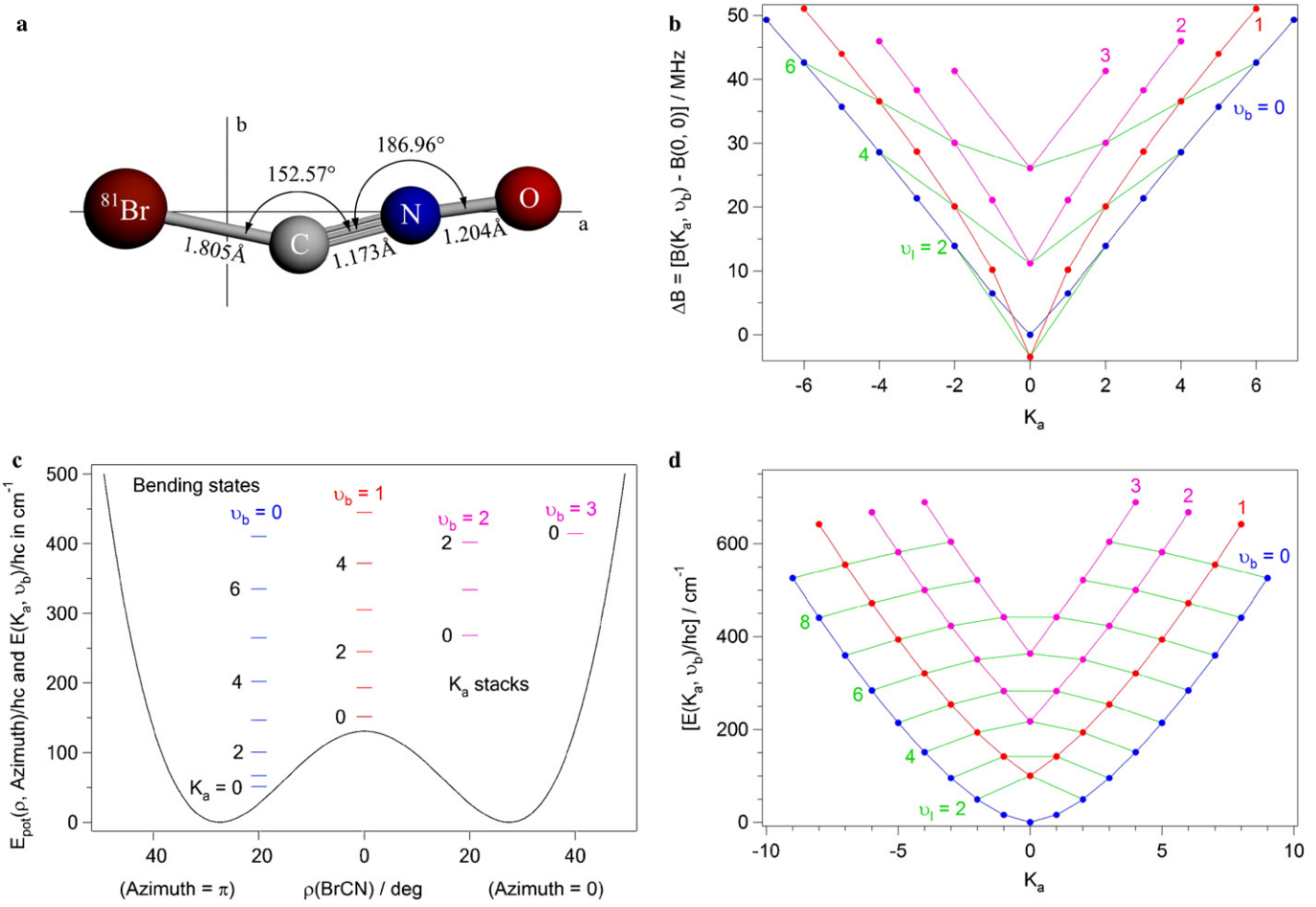

Fig. 14. (a) The structure of BrCNO in the principal axis system is presented with GSRB parameters [26] based in part on *ab initio* values [71]; (b) end-over-end rotational contributions to the energy plotted as ΔB versus K_a; (c) the radial bending potential function for ν_7 based on GSRB calculations [26]; and (d) the two-dimensional bending-rotation term values plotted versus K_a for $J = K_a$. All data plotted are experimentally determined. (For interpretation of the references in colour in this figure legend, the reader is referred to the web version of this article.)

[72] and infrared spectroscopy [61] the band system of the fundamental of the large-amplitude vibration was finally observed directly and studied in great detail. The extremely low wave number of only 18.3 cm^{-1} provides a full separation of the CCC bend from all the other normal modes and gives rise to a complex hot band system which extends over 70 cm^{-1} in the far infrared spectral region [61]. This dense and complex structure is essentially repeated in every band system in the mid infrared region.

In the linear-to-bent correlation diagram given in Fig. 1, no pattern at all can be recognized in the energy manifold for OCCCO. In panels (b) and (d) of Fig. 13 we see the patterns for the end-over-end rotational energy and the bending-rotation energy as a function of the rotational angular momentum quantum number K_a. These energy–momentum maps show an accentuation of what we have observed for HCNO. The ground vibrational state with $K_a = 0$ is just a few cm^{-1} above the monodromy point in the potential surface [42]. SRB fitting of OCCCO data was carried out already in 1980 by Bunker [73] and extended by Jensen and Johns [74,75].

5.5. Bromonitrileoxide, BrCNO, and Chloronitrileoxide, ClCNO

Low-resolution infrared and photoelectron spectroscopy studies in combination with medium-level *ab initio* calculations [78,79] had suggested that the molecules BrCNO and ClCNO might possess highly anharmonic BrCN and ClCN large-amplitude bending modes which would be consistent with the molecular structures displayed in of Figs. 14 (a) and 15 (a). Lichau et al. [26] examined this possibility by reporting the high-resolution rotational spectra for both molecules in the millimeter wave spectral region. The analysis revealed a new category of quasi-linearity. The reduced rotational data for the two molecules are plotted in Figs. 14 (b) and 15 (b). The two-dimensional potential surfaces (see Eq. (6) and Table 1) were derived from the pure rotational data with the help of the GSRB Hamiltonian and are in very good agreement with the high-level *ab initio* calculations of Koput [71,76]. This gave us great confidence in predicting bending-rotation energy levels for higher vibrational states, and for other molecules.

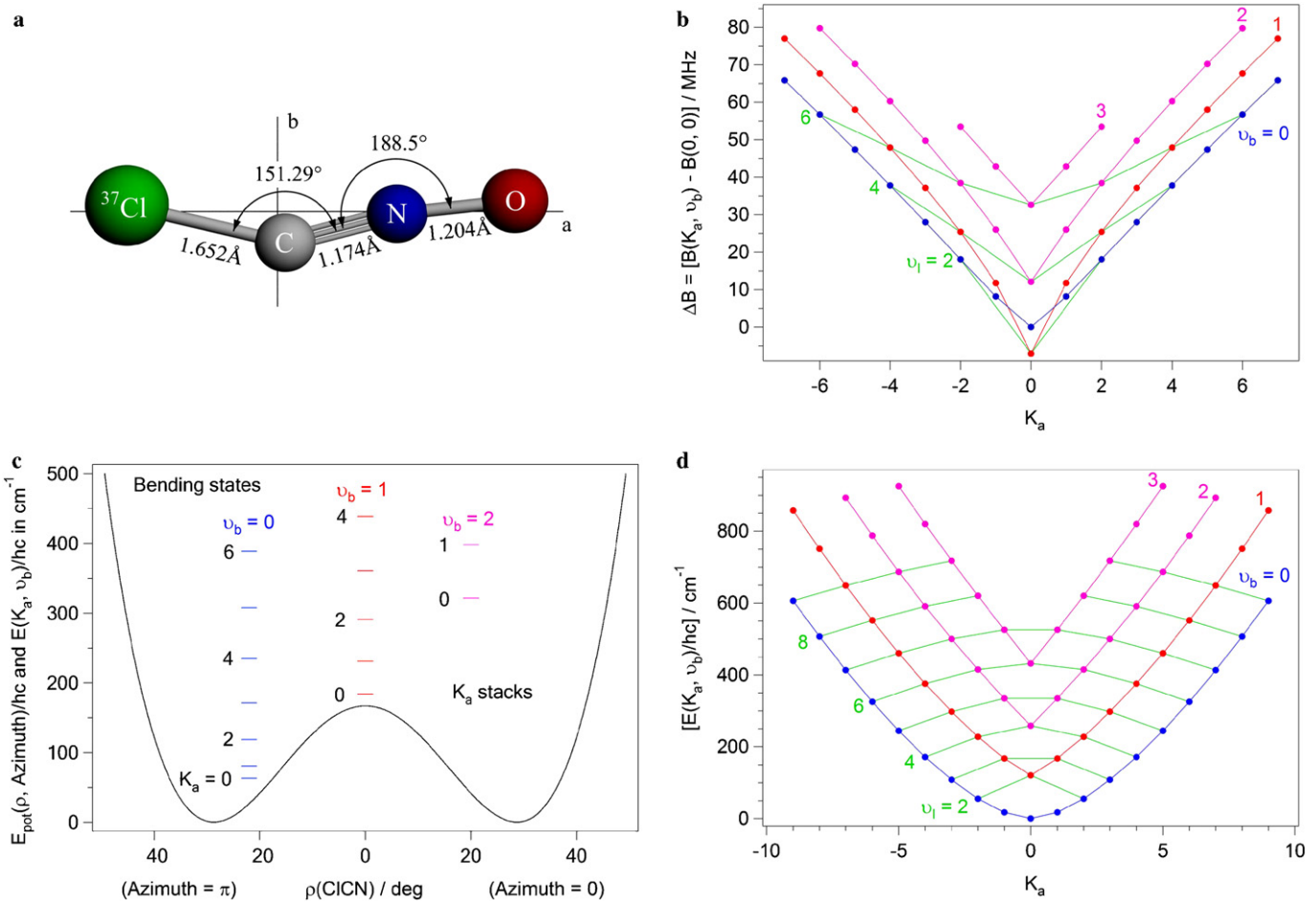

Fig. 15. (a) The structure of ClCNO in its principal axis system is shown with GSRB parameters [26] based in part on *ab initio* values [76]; (b) end-over-end rotational contributions to the energy plotted as ΔB versus K_a; (c) the radial bending potential function for ν_7 [26] based on GSRB calculations; and (d) the two-dimensional bending-rotation term values plotted versus K_a for $J = K_a$. All data plotted are experimentally determined. (For interpretation of the references in colour in this figure legend, the reader is referred to the web version of this article.)

BrCNO and ClCNO show nearly identical spectral properties which can be studied by inspecting Figs. 14 and 15. The levels $K_a = 0$, 1, and 2 of the ground vibrational state for both molecules (indicated in blue) are well below the monodromy point while the levels $K_a = 0$, 1, 2,... for $v_b = 1$ (indicated in red) are above the barrier, and include the $K_a = 0$ level closest to the top or monodromy point. The lowest (blue) curve in panel (d) of each figure is clearly differentiable, while the higher curves (red and pink) are not. Thus, the mathematically predicted effects of quantum monodromy are clearly demonstrated. If we inspect panel (b) for both BrCNO and ClCNO we find the striking property that the end-over-end rotational contributions [$B(K_a,v_b)$ values] to the energy for both molecules have a minimum at $K_a = 0$ for the $v_b = 1$ vibrational state, not the ground state. This was one of reasons why the rotational spectra for these molecules were very hard to assign. An analogous effect was observed earlier by Koput [80,81] in the analysis of the microwave spectrum of CH_3NCS, a quasi-symmetric top molecule, which is further indicative of the fact that we encounter here a robust property of all these molecular quantum systems. These were the first observed cases of a non-monotonic progression of $B(K_a,v_b)$ with vibrational excitation.

5.6. Cyanogen isothiocyanate, NCNCS

At the present state of the investigation of the spectrum of NCNCS only rotational data are available. It is symptomatic that a correct assignment of the microwave data was impossible until model calculations accounting for the large-amplitude bending motion were invoked in the work of King et al. [77] in 1985, which extended only to the ground state and the first three excited states of the large-amplitude CNC bending mode, the first excited state of which lies at $\approx$80 cm^{-1}. The currently available data set now includes millimeter wave rotational transitions in the ground state and five excited bending states [43]. The molecular structure in the principal axis system given in Fig. 16 (a) represents the predicted *ab initio* equilibrium structure of NCNCS. NCNCS was later [22] revisited in a GSRB treatment. We have extended those GSRB calculations up to $v_b = K_a = 12$, and found that for the states assigned so far they predict the values of $E(K_a,v_b)/hc$ within

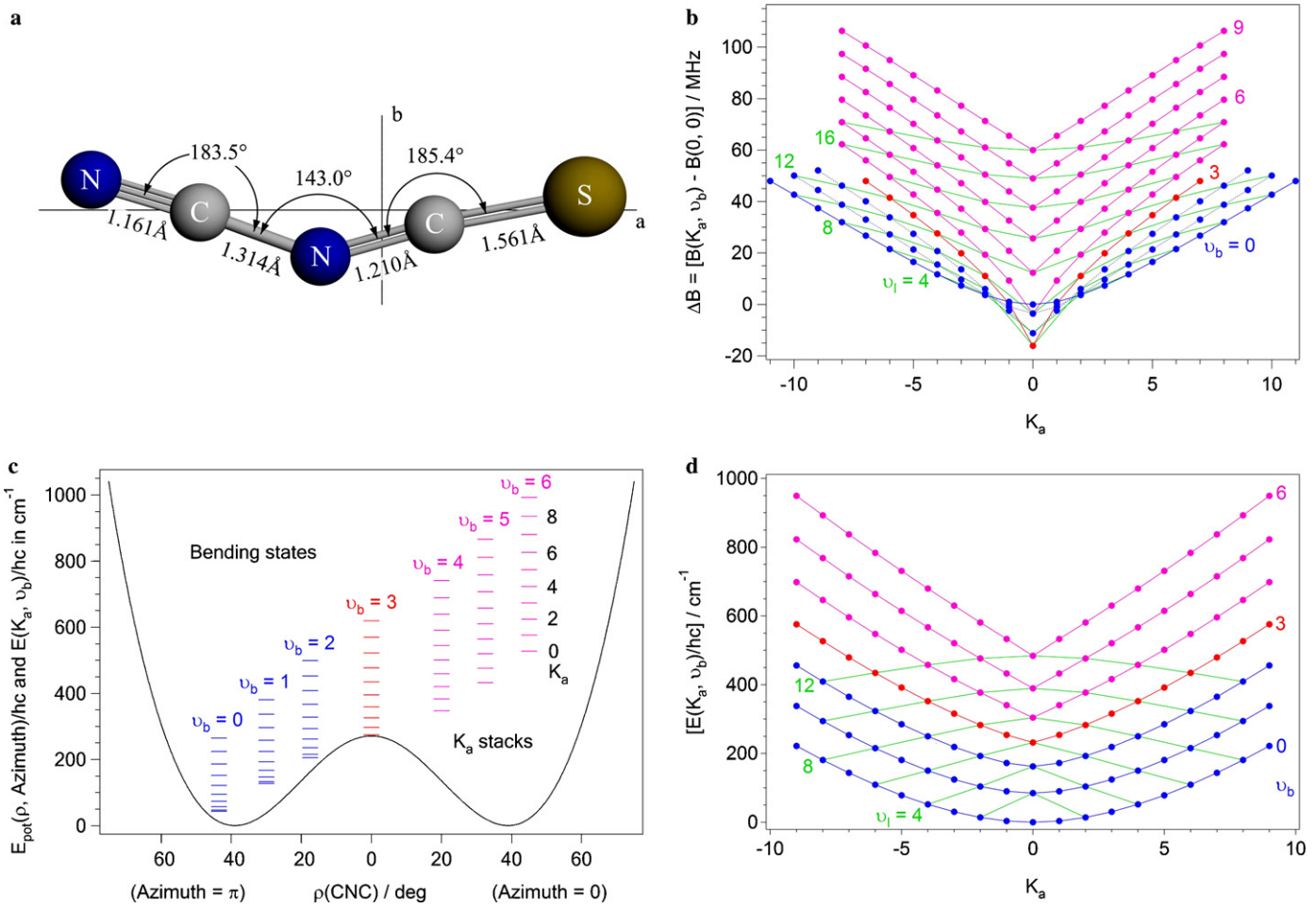

Fig. 16. (a) The structure of NCNCS based on recent high-level *ab initio* calculations [43] is given in the principal axis system; (b) end-over-end rotational contributions to the energy are plotted as ΔB versus K_a; (c) the two-dimensional radial bending potential function for ν_7 (bent numbering) was determined by GSRB least squares fit to the available rotational data [77,22,43]; and (d) the two-dimensional bending-rotation term values plotted versus K_a for $J = K_a$. Points for $v_b \leqslant 5$ are experimentally determined.

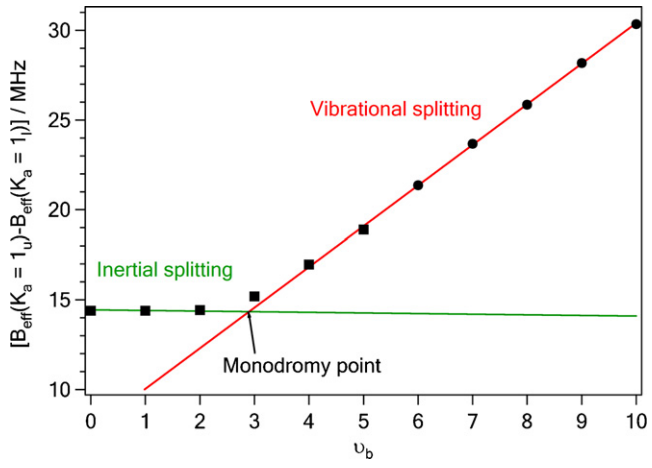

Fig. 17. $K_a = 1$ splitting observed for NCNCS in the ground vibrational state $v_b = 0$ and five higher excited bending state (squares) of the large-amplitude mode ν_7. The abruptness of the transition of the asymmetry splitting of the bent NCNCS molecule to the rotational ℓ-type doubling of linear NCNCS is manifest. The round dots are predicted values.

$1\,\mathrm{cm}^{-1}$, and the $B(K_a,v_b)$ values within a fraction of a MHz, not resolvable in Fig. 16. The potential parameters derived from the microwave data alone are given in Table 1 and define the curve shown in panel (c). Panel (b) shows us the observed ΔB versus K_a. The blue and red curves display the values for NCNCS molecules in the four bending states previously observed, including the ground state, for which $B(K_a,v_b)$ progressively decreases. The pattern changes abruptly with $v_b = 4$, in a manner not previously expected, but precisely predicted. If we inspect the red curve for $v_b = 3$ we see that the $K_a = 0$ level is characterized by the smallest effective rotational constant and therefore the largest effective moment of inertia – and this is just at the total energy corresponding to the monodromy point. As we are now learning, this is a very robust property of quasi-linear molecular systems. If we look at the K_a dependence of bending-rotation energies $E(K_a,v_b)/hc$ [panel (d)] on K_a for the states $v_b > 3$, we observe a close similarity to the energy–momentum plots for the linear molecule OCCCS

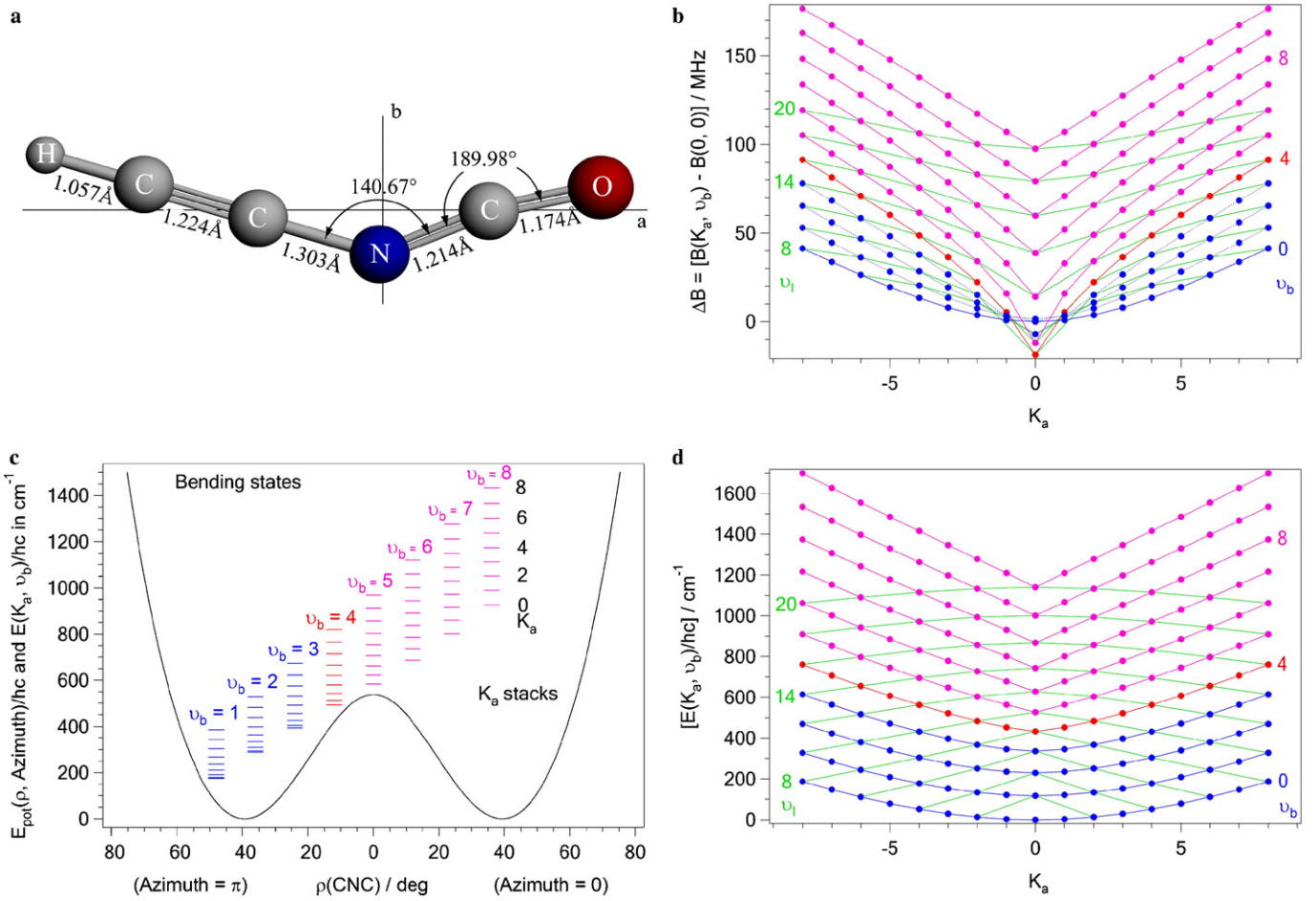

Fig. 18. (a) The structure of HCCNCO displayed in the principal axis system is based on the GSRB analysis [28]; (b) end-over-end rotational contributions to the energy plotted as ΔB versus K_a; (c) the radial bending potential function for the CNC bending mode ν_9 (bent numbering) [82] is based on the GSRB analysis [28]; and (d) the two-dimensional bending-rotation term values plotted versus K_a for $J = K_a$. Points for $v_b \leqslant 3$ are experimentally determined.

shown in Fig. 10, our linear poster-molecule. The curves for $v_b < 3$ in Fig. 16 (d), on the other hand, as will be seen below, resemble those obtained for a clearly bent asymmetric rotor molecule. The quantum monodromy plot in Fig. 16 (d) has precisely the topology that was predicted in the mathematical [11] and theoretical [13–15] work for a system that exhibits quantum monodromy. The smooth and differentiable blue curves associated with the bending state $v_b = 0$, 1, 2, evolve rapidly into a succession of red ($v_b = 3$) and pink curves ($v_b = 4$, 5, 6, ...) with pronounced kinks at $K_a = 0$. The green curves representing the linear notation with ($v_l = 8$, 10, 12,...) become differentiable. Furthermore, as we saw in the detailed view of Fig. 16 (d) given in Fig. 9, the vibrational and rotational unit vectors undergo a skew transformation when carried around the monodromy point, as predicted by the topological theory.

5.6.1. Splitting of levels with $K_a = 1$

In 1942–1943, there was brief controversy between Gerhard Herzberg and Harald Nielsen about the origin of the J-dependent splitting of the $K_a = 1$ ($v_l = 1$, $\ell = 1$) levels of CO_2 and other linear molecules. Herzberg proposed that it was an effective asymmetry splitting, thus due to inertial properties of the molecule [83]. Nielsen saw it as the result of Coriolis interactions between the bending motion and the stretching motions in the molecule [84]. Nielsen's formulation proved to reproduce the splittings, known as ℓ-type doubling, but a close correlation between the two explanations was recognized. The dependence of this splitting on bending excitation differs fundamentally in the two limiting cases, however. Is there a gradual transition from one form to the other? Can we find a simple closed expression which will at least roughly describe this splitting across the entire range from linear to bent? These were questions we asked earlier. The data for NCNCS shows the answer. For Fig. 16 we averaged the two measured values of ΔB to give one value for $K_a = 1$. If we now plot the energy interval represented by the difference between the same two effective $B(K_a = 1, v_b)$ values, as in Fig. 17 for NCNCS, we see a very simple curve. We learn immediately from this plot, first, that there is no one simple

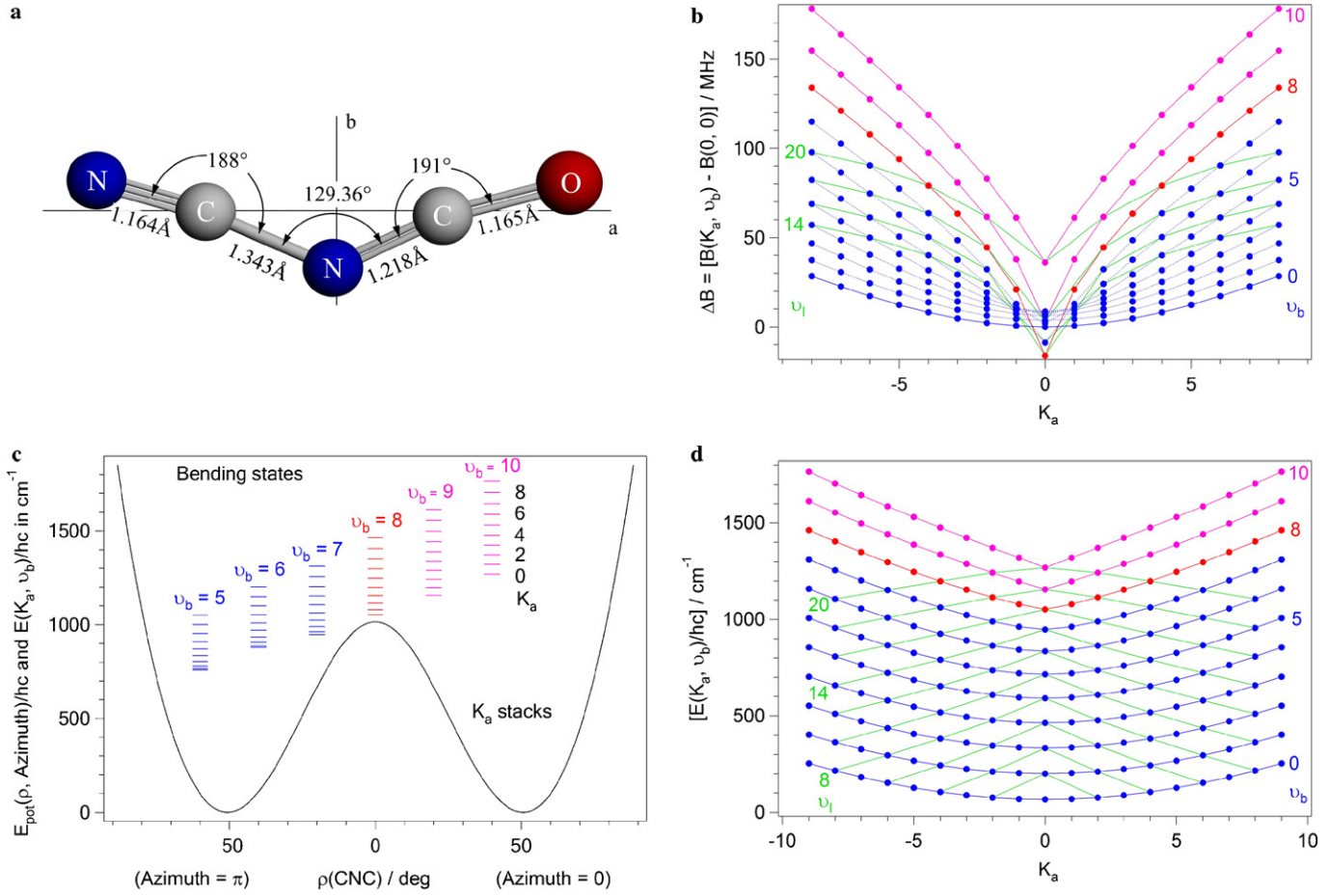

Fig. 19. (a) The structure of NCNCO given here refers to the GSRB parameters [22], which are based on the early microwave work [85,86]. The molecule is displayed in the principal axis system; (b) end-over-end rotational contributions to the energy plotted as ΔB versus K_a; (c) the radial bending potential function for ν_7 (bent numbering) [22]; and (d) the two-dimensional bending-rotation term values plotted versus K_a for $J = K_a$. Points for $v_b \leqslant 3$ are experimentally determined.

closed expression that will represent the splitting, and second, there is a remarkably swift transition from the almost negligible v_b dependence typical for a bent molecule to the strong linear dependence expected for a linear molecule.

In the bent limiting case, the splitting can be well approximated by $(B_{v_b} - C_{v_b})/2$, where B and C are obtained for each v_b from an asymmetric rotor fit to the rotational transitions. The vibrational dependence on v_b is very small, since it is the difference between the (usually similar, for this type of molecule) vibrational variations of B_{v_b} and C_{v_b}. The term linear in v_b is only about one percent of the ground state splitting. For the bent case, the splitting is thus an inertial effect, and the splitting is nearly constant upon vibrational excitation. This is just what we see for $v_b = 0$, 1, and 2 of NCNCS. For states above the monodromy point, the splitting is indeed dominated by Coriolis interactions of the bending mode with the stretching modes of the neighboring bonds. It is a vibrational effect; it is dominated by a substantial term linear in $(v_b + 1)$, with a modest constant term, a left-over from the phase space below the monodromy point. For a linear molecule like OCCCS, the constant term is entirely negligible. As we see in Fig. 17, the transition from the bent to the linear behavior is effected within a range of no more than three vibrational states: The state closest to the critical point, and the two adjacent states.

The equivalent plots for the other species presented here look like excerpts or extrapolations of this plot, with the critical point occurring at lower or higher v_b, in direct relation to the location of the monodromy point. In terms of molecular dynamics, this abrupt shift in the mathematical description of the dynamics is fully in keeping with the perspective of quantum monodromy in this family of molecules. For these molecules, Herzberg and Nielsen were both right.

5.7. Ethynyl isocyanate, HCCNCO

For HCCNCO, as for NCNCS, the assignment of the microwave data by Ross et al. [28] required the use of a large-amplitude theoretical model. In the case of HCCNCO this was a GSRB treatment which eventually

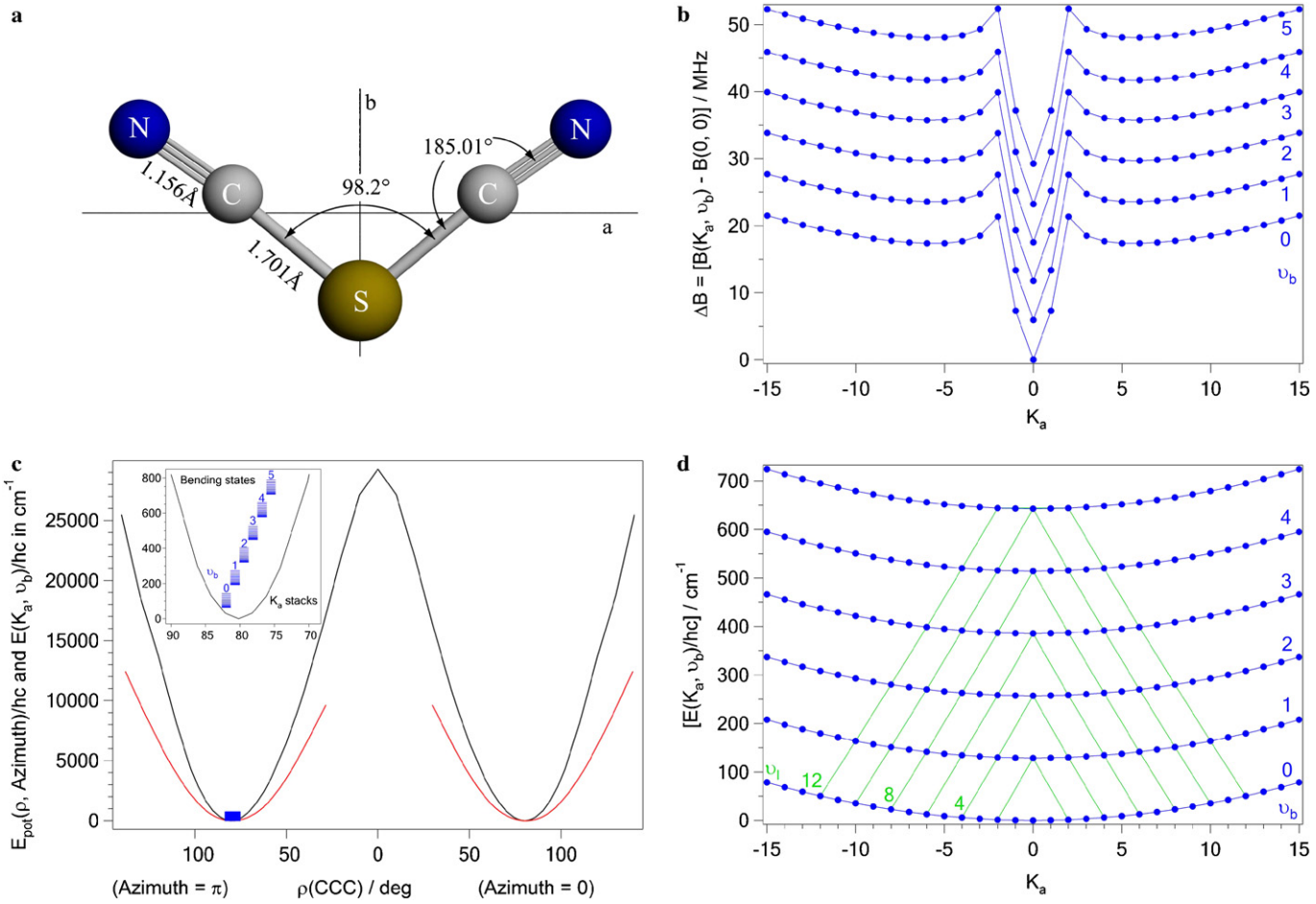

Fig. 20. (a) The structure of $S(CN)_2$ determined in the early microwave work [87,88] and shown in the principal axis system; (b) end-over-end rotational contributions to the energy plotted as ΔB versus K_a based on the work of Kisiel and coworkers [44]; (c) in blue, the radial bending potential function for ν_4 (bent numbering) [44,88], and in red, the GSRB fit to a cubic spline function (see Section 3); and (d) the two-dimensional bending-rotation term values plotted versus K_a for $J = K_a$ [44]. Points for $v_b \leqslant 5$ are experimentally determined.

incorporated the microwave spectrum of the ground and the first three excited vibrational states of the large-amplitude CNC bending mode. This treatment resulted in the quantitative determination of the molecular structure presented in Fig. 18 (a) and the two-dimensional potential function [see Eq. (6) and Table 1] shown in panel (c). The data and original calculation only extend up through $v_b = 3$, just as in the case of the microwave data for NCNCS prior to the present experimental work. However, we gained confidence in the predictive capability of the GSRB from the accuracy of the predictions for higher v_b confirmed by our NCNCS work and therefore we have extended the calculations, as in the case of NCNCS, up to $v_b = K_a = 10$. The corresponding rotation-bending term values $E(K_a, v_b)$ are plotted versus K_a as an energy–momentum map and displayed in panel (d). Inspection of the red curve for the bending state $v_b = 4$ reveals, as in the case of NCNCS, a kink at $K_a = 0$, but it is not as pronounced as in the previous example. However, the end-over-end rotational contributions plotted in panel (b) reveal without doubt that the red curve for $v_b = 4$ exhibits the smallest $\Delta B(K_a,v_b)$ value at $K_a = 0$. In this particular molecule the energy levels with $K_a = 0$ and $v_b = 4$ and 5 just about straddle the classical monodromy point, as is shown in panel (c). The pink curves in panel (b) and (d) for the bending states $v_b = 6$, 7, 8, 9, 10 are clearly above the classical monodromy point and therefore reveal the evolution of the end-over-end rotational energy–momentum map from that of a bent molecule to that of a linear molecule.

5.8. Cyanogen isocyanate, NCNCO

This molecule has a very different potential function from that of its isomer NCCNO, discussed in Section 5.2. Fig. 19 shows that it has a rather strongly bent equilibrium angle and a high barrier to linearity [see Eq. (6) and Table 1]. The currently available experimental data [85,86] only extend up through $v_b = 3$, as in the case of the microwave data for NCNCS and HCCNCO. Again, we have extended the GSRB calculations up to $v_b = K_a = 10$ and plotted in panels (b) and (d) of

Fig. 19 the experimental and predicted effective ΔB values and the predicted bending-rotation term values. Both plots show that the critical point is close to the $K_a = 0$ level of the $v_b = 8$ bending state, which is just the situation found recently for water [20], confirming predictions of Child et al. [13–15]. While the plot displayed in panel (d) of Fig. 19 confirms our expectations, the plot of $B(K_a,v_b)$ vs K_a given in panel (b) is more remarkable. We see that the $B(K_a = 0, v_b)$ value in the first few bending states, below the top of the barrier, initially increases from the ground state, as in the normal case for a bent molecule, but then for low K_a it plunges into a minimum which totally overwhelms the tendency to increase with increasing excitation, and finally rises abruptly, above the monodromy point, to resume its upwards trend but now in a pattern characteristic of a linear molecule.

Although the extrapolation of the predicted eigenvalues up to the critical point is farther for NCNCO than for HCCNCO, we are confident that the pattern is correctly predicted, and that the experimental energy levels and $B(K_a,v_b)$ values will be found to lie within a few wave numbers or MHz, respectively, of the predicted values. As in the case of water, interactions with other excited vibrational states will of course complicate the picture.

5.9. Sulfur dicyanide, $S(CN)_2$

As can be seen from Fig. 20 or Table 1, there is a substantial gap between the potential functions for NCNCO and the truly bent limiting case, represented here by $S(CN)_2$, an isomer of NCNCS. As we started this work, there was only an imprecise indication of the bending fundamental from IR data [89,88], and very limited microwave data in the ground state [87,88]. Recent millimeter wave measurements, to be reported in detail elsewhere [44], have provided rotational data for $v_b = 0$–5, enough to allow a GSRB calculation (see Section 3) which arrives at a potential roughly consistent with that yielded by *ab initio* calculations [44]; both curves are plotted in Fig. 20. (The rotational data is fit far more satisfactorily with six effective Watson Hamiltonians for the six vibrational states.) Intensity measurements in the rotational spectrum give an experimental estimate of the vibrational quanta. A deep and narrow potential well defines the small-amplitude vibration of a bent molecule. The energy–momentum plot of $E(K_a, v_b)/hc$, shows a set of perfectly smooth, differentiable parabolas, entirely dominated by the vibrational quanta in v_b and the much smaller parabolic rotational contribution AK_a^2. The plot of ΔB versus K_a in panel (b) shows a new element: for low K_a, there is a zigzag pattern which is typical of the rotational structure in the spectrum of near-prolate asymmetric rotor molecules [90]. This is superimposed on the gentle parabola described by the centrifugal distortion parameter D_{JK}. The zigzag pattern is not related to monodromy, but to the $\Delta K_a = 2$ interactions in an asymmetric rotor. Actually, this pattern overlays each of the ΔB versus K_a plots of the lowest v_b states of the last five species treated above, which can be analyzed, if with poor results, as asymmetric rotor molecules. However, this contribution to the pattern is far smaller for all of the above species than the resolution of the plots shown here, and is in addition partially quenched by the proximity of adjacent vibrational levels. In $S(CN)_2$, the height of the barrier relative to the vibrational quanta, the large ratio of the vibrational quanta to $B(K_a, v_b)$, and the asymmetry parameter $\kappa = -0.84773$, as opposed to the value of $\kappa = -0.99938$ for the ground state of NCNCS, $\kappa = -0.99865$ for HCCNCO and $\kappa = -0.99718$ for NCNCO, ensure that the pattern due to asymmetry dominates the rotational end-over-end energy. This, then, is the signature of a truly bent molecule.

6. Conclusion

As has been shown in Section 5, the classical monodromy point of the punt in a champagne bottle potential can be associated in the quantum world with a $K_a = 0$ energy level (or two levels) nearest to it and introduces a quantum lattice defect that leads to robust properties of quantum monodromy in the spectra of quasi-linear molecules.

With the data now available for the molecules discussed here, and with the help of the GSRB Hamiltonian to provide realistic predictions based on these data, we have a rather complete picture of what to expect from the spectra of molecules that have in their two-dimensional anharmonic potential surface a critical or monodromy point in the range of excitation that is accessible experimentally. The bending vibrational energy–momentum maps for the molecules BrCNO (see Fig. 14), ClCNO (see Fig. 15), NCNCS (see Fig. 9 and Fig. 16), HCCNCO (see Fig. 18) and NCNCO (see Fig. 19) show beyond doubt the existence of quantum monodromy. The anharmonic component of the potential function for NCCNO, HCNO and OCCCO causes distortions of the energy/momentum map that form a smooth progression from the harmonic oscillator to the champagne bottle potential. In addition, a dramatic effect of quantum monodromy on the end-over-end rotational energy of quasi-linear molecules is clearly demonstrated for all quasi-linear molecules discussed: The $K_a = 0$ energy level closest to the monodromy point exhibits a strong local minimum of the rotational constant (a local maximum of the relevant moment of inertia). This property is absolutely robust and must underly the spectral pattern for the water molecule and various other species generally considered bent. In order to illuminate further this manifestation of quantum monodromy in the rotational constant we show for the molecules NCNCS (Fig. 21), HCCNCO (Fig. 22) and NCNCO (Fig. 23) three-dimensional images of their respective quantum lattices composed of ΔB values as functions of K_a and v_b. The systematic progression in the location of the minimum and the characteristic shape of the deformity that travels with it are a revelation.

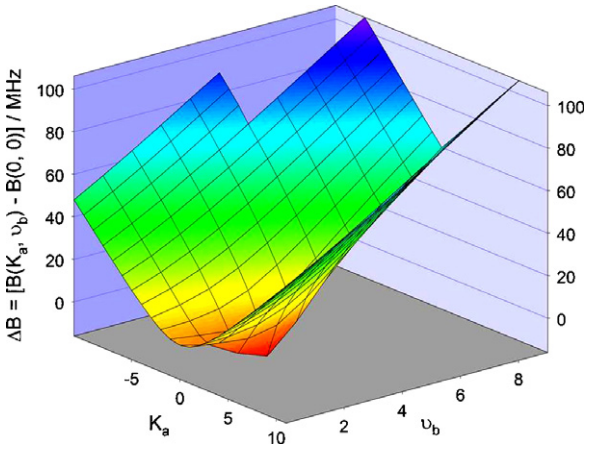

Fig. 21. Three-dimensional image of the quantum lattice for the end-over-end energy contribution plotted as $\Delta B(K_a,v_b)$ versus K_a and v_b for the molecule NCNCS. The data points beyond $v_b = 5$ are predicted by the GSRB Hamiltonian.

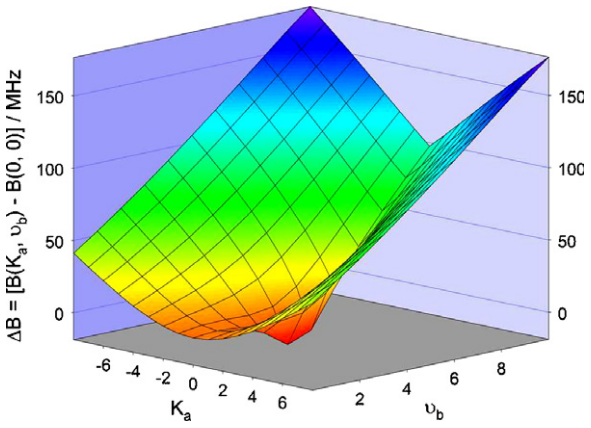

Fig. 22. Three-dimensional image of the quantum lattice for the end-over-end energy contribution plotted as $\Delta B(K_a,v_b)$ versus K_a and v_b for the molecule HCCNCO. The data points beyond $v_b = 3$ are predicted by the GSRB Hamiltonian.

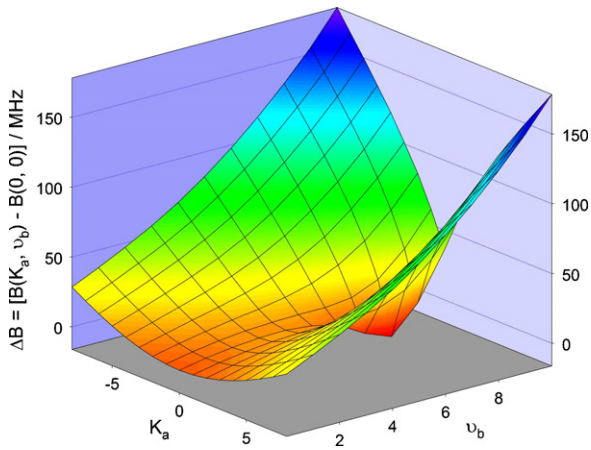

Fig. 23. Three-dimensional image of the quantum lattice for the end-over-end energy contribution plotted as $\Delta B(K_a,v_b)$ versus K_a and v_b for the molecule NCNCO. The data points beyond $v_b = 3$ are predicted by the GSRB Hamiltonian.

These surfaces should be invaluable for the understanding and assignment of rotational and rovibrational spectra of quasi-linear molecules in all spectral regions. The non-monotonic dependence of $B(K_a = 0,v_b)$ on v_b was simply not foreseen.

The minimum in the $B(K_a,v_b)$ values is related to the probability-density distribution of the wave functions. The probability-density close to the linear configuration can become substantial for $K_a = 0$ as the energy approaches the critical point [91]. Since it became conventional to plot only radial probability distribution, which must go to zero at $\rho = 0$ due to the definition of the differential metric, this fact has been widely overlooked. Since the moment of inertia reaches a maximum with the molecule extended, this means the rotational constant $B(K_a,v_b)$ will reach a local minimum at the $K_a = 0$ level closest to this energy.

Due to the uncertainty inherent in quantum mechanics the transition from the realm below the critical point to the realm above it is softened. Thus the minimum in $B(K_a,v_b)$ can also occur for a $K_a = 0$ level just below the monodromy point, as is the case in HCCNCO. Quantum monodromy in a champagne bottle potential can be considered a 1:(−1) resonance [36].

We now can confidently predict the qualitative structure of the energy level manifold of essentially any bending mode in isolation. In general, as in H_2O or HCNO, the large-amplitude bending mode is seldom well separated from the other vibrational modes, and the simplicity and symmetry of the energy–momentum plots shown here will not be easy to see. However, these patterns determine the unperturbed pattern of large-amplitude bending modes that interact with the small-amplitude modes of all real molecules.

During the course of this work we realized that the availability of excellent tools, that is both Hamiltonians and computers, to numerically fit our data had blinded us to the hidden beauty and symmetry of the invariants of the dynamic systems we were studying. Furthermore, chemical physicists, spectroscopists, theoretical physicists, chemists, and mathematicians have their own terminology, concepts and tools that make it difficult to pass concepts from one field into the other. Therefore we agree with Sadovskiĭ and Zhilinskiĭ [36] that a collaborative effort should be made to overcome these barriers in the study of monodromy in molecular systems.

Acknowledgments

This paper is dedicated to Gisbert Winnewisser on the occasion of his 70th birthday. In particular Brenda and Manfred note that more than 40 years have elapsed since our joint stay in Walter Gordy's Microwave Laboratory at Duke University. We have shared many scientific endeavors with Gisbert. Our collaborations intensified after Gisbert returned to Germany and accepted a position at the Max Planck Institute for Radioastronomy and later with the University of Cologne. We always resonated with

his boundless enthusiasm for new discoveries, his deep interest in molecules, and his farsightedness in the development of advanced technology for millimeter wave, sub-millimeter wave and Terahertz physics and radioastronomy. We thank Z. Kisiel for making essential results of his analysis of $S(CN)_2$ data available before publication and for many thoughtful discussions. We thank J. Tennyson and M. Child for discussions stimulating our renewed efforts to understand these spectra. The authors thank Jacek Koput for valuable comments. The experimental work at OSU is supported by the Army Research Office, the GSRB work at UNB is supported by the Natural Sciences and Engineering Research Council of Canada (NSERC). The mathematical work at UC is partially supported by NSERC.

References

[1] R.N. Dixon, Trans. Faraday Soc. 60 (1964) 1363.
[2] J.W.C. Johns, Can. J. Phys. 45 (1967) 2639.
[3] W.R. Thorson, I. Nakagawa, J. Chem. Phys. 33 (1960) 994.
[4] K. Yamada, M. Winnewisser, Z. Naturforsch. 31A (1976) 139.
[5] J.T. Hougen, P.R. Bunker, J.W.C. Johns, J. Mol. Spectrosc. 34 (1970) 136.
[6] B.P. Winnewisser, Chapter 6 of Molecular Spectroscopy: Modern Research vol. 3 (1985) 321.
[7] W. Quapp, B.P. Winnewisser, J. Math. Chem. 14 (1993) 259.
[8] N.N. Nekhoroshev, Trans. Moskow Math. Soc. 26 (1972) 180.
[9] J.J. Duistermaat, Comm. Pure and Appl. Math. 33 (1980) 687.
[10] R. Cushman, Centrum voor Wiskunde en Informatica Newsletter 1 (1983) 4.
[11] L.M. Bates, J. Appl. Math. Phys. (ZAMP) 42 (1991) 837.
[12] R. Cusham, J.J. Duistermaat, Bull. Am. Math. Soc. 19 (1988) 475.
[13] M.S. Child, T. Weston, J. Tennyson, Mol. Phys. 96 (1999) 371.
[14] M.S. Child, J. Phys. A: Math. Gen. 31 (1998) 657.
[15] M.S. Child, J. Mol. Spectrosc. 210 (2001) 157.
[16] P.R. Bunker, B.M. Landsberg, J. Mol. Spectrosc. 67 (1977) 374.
[17] A.R. Hoy, P.R. Bunker, J. Mol. Spectrosc. 52 (1974) 439.
[18] P.R. Bunker, J.M.R. Stone, J. Mol. Spectrosc. 41 (1972) 310.
[19] P. Jensen, J. Mol. Spectrosc. 128 (1988) 478.
[20] N.F. Zobov, S.V. Shirin, O.L. Polyansky, J. Tennyson, P.F. Coheur, P.F. Bernath, M. Carleer, R. Colin, Chem. Phys. Lett. 414 (2005) 193.
[21] S.C. Ross, T.J. Butenhoff, E.A. Rohlfing, C.M. Rohlfing, J. Chem. Phys. 100 (1994) 4110.
[22] S.C. Ross, J. Mol. Spectrosc. 132 (1988) 48.
[23] W.W. Harper, J. Karolczak, D.J. Clouthier, S.C. Ross, J. Chem. Phys. 103 (1995) 883.
[24] M. Niedenhoff, K.M.T. Yamada, G. Winnewisser, S.C. Ross, J. Mol. Struct. 352/353 (1995) 423.
[25] S.C. Ross, M. Niedenhoff, K.M.T. Yamada, J. Mol. Spectrosc. 164 (1994) 432.
[26] H. Lichau, C.W. Gillies, J.Z. Gillies, S.C. Ross, B.P. Winnewisser, M. Winnewisser, J. Phys. Chem. A 105 (2001) 10065.
[27] H. Lichau, S.C. Ross, M. Lock, S. Albert, B.P. Winnewisser, M. Winnewisser, F.C. De Lucia, J. Phys. Chem. A 105 (2001) 10080.
[28] S.C. Ross, T.A. Cooper, S. Firth, H.W. Kroto, D.R.M. Walton, J. Mol. Spectrosc. 152 (1992) 152.
[29] S.C. Ross, J. Mol. Spectrosc. 161 (1993) 102.
[30] J.R. Dunlop, J. Karolczak, D.J. Clouthier, S.C. Ross, J. Phys. Chem. 95 (1991) 3063.
[31] J.R. Dunlop, J. Karolczak, D.J. Clouthier, S.C. Ross, J. Phys. Chem. 95 (1991) 3045.
[32] F.J. Lovas, R.D. Suenram, S. Ross, M. Kłobukowski, J. Mol. Spectrosc. 123 (1987) 167.
[33] T. Barrow, R.N. Dixon, G. Duxbury, Mol. Phys. 27 (1974) 1217.
[34] P.R. Bunker, B.M. Landsberg, B.P. Winnewisser, J. Mol. Spectrosc. 74 (1979) 9.
[35] R. Escribano, P.R. Bunker, Chem. Phys. Lett. 143 (1988) 439.
[36] D.A. Sadovskiĭ and B.I. Zhilinskiĭ, Mol. Phys., in press .
[37] M. Child, Adv. Chem. Phys., in press .
[38] K. Efstathiou, Metamorphoses of Hamiltonian Systems with Symmetries, Lecture Notes in Mathematics, Springer Verlag, 2005.
[39] R. Cushman, L. Bates, Global Aspects of Classical Integrable Systems, Birkhäuser, 1997.
[40] V.I. Arnold, Mathematical Methods of Classical Mechanics, Springer-Verlag, 1984.
[41] P. Jensen, J. Mol. Spectrosc. 101 (1983) 422.
[42] J. Koput, Chem. Phys. Lett. 320 (2000) 237.
[43] B.P. Winnewisser, M. Winnewisser, I.R. Medvedev, M. Behnke, F.C. De Lucia, S.C. Ross, J. Koput, Phys. Rev. Lett. 95 (2005) 243002.
[44] O. Dorosh, Z. Kisiel, I.R. Medvedev, M. Behnke, M. Winnewisser, F.C. De Lucia, and E. Herbst, J. Mol. Spectrosc. (2006) to be published .
[45] J. Śniatycki, Geometric Quantization and Quantum Mechanics, No. 30 in Applied Mathematical Sciences, Springer-Verlag, 1980.
[46] K. Efstathiou, M. Joyeux, D.A. Sadovskiĭ, Phys. Rev. A 69 (2004) 032504.
[47] S.V. Ngöc, Commun. Math. Phys. 203 (1999) 465.
[48] N.T. Zung, Diff. Geom. Appl. 7 (1997) 123.
[49] B. Zhilinskiĭ, Topology in Condensed Matter. Springer Series in Solid-State Sciences. vol. 150 (2006) 165.
[50] M. Winnewisser, E.W. Peau, Acta Physica. Hungarica. 55 (1984) 33.
[51] M. Winnewisser, J.J. Christiansen, Chem. Phys. Lett. 37 (1976) 270.
[52] M. Winnewisser, E.W. Peau, K. Yamada, J.J. Christiansen, Z. Naturforsch. A 36 (1981) 819.
[53] M. Winnewisser, F. Holland, Astron. Astrophys. 157 (1986) 19.
[54] M. Winnewisser, H. Lichau, F. Wolf, J. Mol. Spectrosc. 202 (2001) 155.
[55] M. Winnewisser, E.W. Peau, Chem. Phys. 71 (1982) 377.
[56] F.M. Nicolaisen, J.J. Christiansen, J. Mol. Struct. 52 (1979) 157.
[57] F. Holland, M. Winnewisser, J.W.C. Johns, Can. J. Phys. 68 (1990) 435.
[58] V. Wagener, M. Winnewisser, M. Bellini, J. Mol. Spectrosc. 176 (1996) 425.
[59] M. Winnewisser, H.K. Bodenseh, Z. Naturforsch. 22a (1967) 1724.
[60] H.W. Kroto, Molecular Rotation Spectra, John Wiley and Sons, 1975.
[61] J.V. Auwera, J.W.C. Johns, O.L. Polyanski, J. Chem. Phys. 95 (1991) 2299.
[62] Th. Brupbacher, R.K. Bohn, W. Jäger, M.C.L. Gerry, T. Pasinszki, N.P.C. Westwood, J. Mol. Spectrosc. 181 (1997) 316.
[63] M. Winnewisser, H.K. Bodenseh, Z. Naturforsch. 22a (1967) 1724.
[64] B.P. Winnewisser, M. Winnewisser, F. Winther, J. Mol. Spectrosc. 51 (1974) 65.
[65] K. Yamada, B.P. Winnewisser, M. Winnewisser, J. Mol. Spectrosc. 56 (1975) 449.
[66] K. Islami, W. Jabs, J. Preusser, M. Winnewisser, B.P. Winnewisser, Ber. Bunsenges. Phys. Chem. 99 (1995) 565.
[67] G. Schulze, O. Koja, B.P. Winnewisser, M. Winnewisser, J. Mol. Struct. 517–518 (2000) 307.
[68] J. Koput, B.P. Winnewisser, M. Winnewisser, Chem. Phys. Lett. 255 (1996) 357.
[69] N.C. Handy, C.W. Murray, R.D. Amos, Philos. Mag. B 69 (1994) 755.
[70] S. Albert, M. Winnewisser, B.P. Winnewisser, Ber. Bunsenges. Phys. Chem. 100 (1996) 1876.
[71] J. Koput, J. Phys. Chem. A 103 (1999) 2170.
[72] E.N. Karyakin, A.F. Krupnov, S.M. Shapin, J. Mol. Spectrosc. 94 (1982) 283.
[73] P.R. Bunker, J. Mol. Spectrosc. 80 (1980) 422.
[74] P. Jensen, J. Mol. Spectrosc. 104 (1984) 59.
[75] P. Jensen, J.W.C. Johns, J. Mol. Spectrosc. 118 (1986) 248.
[76] J. Koput, J. Phys. Chem. A 103 (1999) 6017.

[77] M.A. King, H.W. Kroto, B.M. Landsberg, J. Mol. Spectrosc. 113 (1985) 1.
[78] T. Pasinszki, N.P.C. Westwood, J. Phys. Chem. A 99 (1995) 6401.
[79] T. Pasinszki, N.P.C. Westwood, J. Phys. Chem. A 102 (1998) 4939.
[80] J. Koput, J. Mol. Spectrosc. 118 (1986) 189.
[81] J. Koput, J. Mol. Spectrosc. 118 (1986) 448.
[82] T. Pasinszki, B. Havasi, Phys. Chem. Chem. Phys. 5 (2003) 259.
[83] G. Herzberg, Rev. Mod. Phys. 14 (1942) 219.
[84] Harald H. Nielsen, Wave H. Shaffer, J. Chem. Phys. 11 (1943) 140.
[85] W.H. Hocking, M.C.L. Gerry, J. Mol. Spectrosc. 59 (1976) 338.
[86] B. Bak, H. Svanholt, A. Holm, Acta Chem. Scand. A 33 (1979) 597.
[87] W. Arnold, H. Dreizler, H.D. Rudolph, Z. Naturforsch. 19a (1964) 1428.
[88] L. Pierce, R. Nelson, C. Thomas, J. Chem. Phys. 43 (1965) 3423.
[89] F. Cataldo, Polyhedron 19 (2000) 681.
[90] K. Yamada, M. Winnewisser, Z. Naturforsch. 30a (1975) 672.
[91] J.A. Duckett, PhD thesis, University of Reading, Reading, England, (1976).